Carbon Trends 23 (2026) 100651

Contents lists available at ScienceDirect

Carbon Trends

journal homepage: www.elsevier.com/locate/cartre

Design and evaluation of a low-cost pyrolysis reactor for biomass valorization: temperature-dependent structural evolution of biochar

Ishraque Mashiat [a], Alif Al Arefin Prodhan [b,*], Md. Mahbub Alam [c], Md. Mukhlesur Rahman [c], Md. Khairul Hassan Bhuiyan [d], Md. Kamrul Hasan Fakir [e]

[a] Department of Architecture, Ahsanullah University of Science and Technology, Dhaka-1208, Bangladesh
[b] Institute of Water and Flood Management, Bangladesh University of Engineering and Technology, Dhaka-1000, Bangladesh
[c] Department of Animal Science, Bangladesh Agricultural University, Mymensingh-2202, Bangladesh
[d] Department of Physics, Bangladesh Agricultural University, Mymensingh-2202, Bangladesh
[e] Materials Science Division, Atomic Energy Centre, Dhaka-1000, Bangladesh

ARTICLE INFO

Keywords:
Slow pyrolysis
Laboratory-scale reactor
Decentralized biomass valorization
Biochar characterization
Waste-to-resource

ABSTRACT

Affordable, laboratory-scale pyrolysis reactors are scarce in developing countries, constraining decentralized biomass valorization. This study presents the engineering design, fabrication, and performance evaluation of a low-cost, slow pyrolysis batch reactor for academic research and small-scale rural applications. The reactor was modeled in SketchUp and fabricated locally, with a controlled operational design capacity of 1000 °C, and an experimentally validated operating window of 450–700 °C. Total construction cost was USD 557.02 and average biochar operating energy cost was USD 0.37 per kg, comparing favorably with other reported low-cost and pilot-scale systems. Four feedstocks, poultry manure, bones, rice husk, and wood flakes were converted into biochar with yields range of 14.8–43 wt.% depending on feedstock and temperature. Detailed characterization of poultry manure biochar at 450 °C and 600 °C revealed temperature-driven attenuation of oxygen-containing functional groups (Fourier-transform infrared spectroscopy, FTIR), a transition from amorphous to turbostratic carbon (X-ray diffraction, XRD), apparent surface roughening and pore enlargement (scanning electron microscopy, SEM; qualitative only), and a reduction in total heavy metal concentrations within International Biochar Initiative (IBI) threshold limits (inductively coupled plasma mass spectrometry, ICP-MS). The condensed liquid by-product was predominantly aqueous, indicating limited fuel potential. Short-term field application to two rice varieties produced statistically significant effects only on shoot and total biomass at the milking stage of BRRI Dhan-88. Combining multi-feedstock processing, condensate recovery, and integrated FTIR, XRD, SEM, and ICP-MS characterization within a single locally fabricated platform, the reactor offers a reproducible, low-cost pathway for biomass residue valorization in resource-constrained locations.

1. Introduction

With the rapid expansion of both small-scale and large-scale agricultural and livestock industries worldwide, the amount of produced biomass wastes has increased substantially in recent years [1]. If mismanaged, improperly disposed of, or left untreated, these wastes can cause environmental pollution, soil degradation, surface and groundwater contamination, and greenhouse gas emissions [2,3]. To address these challenges, production of value-added and environmentally friendly materials, such as biochar, has emerged as a sustainable waste management approach, attracting significant research attention [4,5].

Pyrolysis is one of the various thermochemical conversion processes, in which, biomass is converted into biochar (solid fraction), bio-oil (condensed liquid fraction), and syngas (non-condensed fraction), in absence of, or under limited oxygen [6–11]. Slow pyrolysis process, which has heating rate of 0.07–0.33 °C/s, operating temperature of 300–900 °C, and solid residence time of 1–740 min [51], is applied in this study.

Biochar is a carbon-rich solid that can improve soil fertility through enhanced soil microbial activity, water retention, carbon sequestration,

* Corresponding author.
E-mail addresses: ishraquemashiat19@gmail.com (I. Mashiat), anandaprodhan@gmail.com (A.A.A. Prodhan), mahbub.alam.bau16@gmail.com (Md.M. Alam), mmrahman.as@bau.edu.bd (Md.M. Rahman), bhuiyan.phy@bau.edu.bd (Md.K.H. Bhuiyan), kh210071@gmail.com (Md.K.H. Fakir).

https://doi.org/10.1016/j.cartre.2026.100651
Received 4 April 2026; Received in revised form 4 May 2026; Accepted 7 May 2026
Available online 12 May 2026

and contaminant immobilization, while also offering applications in water purification, energy storage, catalyst or photocatalyst production, wastewater treatment, and electrode material development for lithium-ion batteries [12–19]. Beyond these, Biomass-derived carbonaceous materials have potential for sustainable composite and film applications by improving mechanical performance, thermal behavior, degradability, and electromagnetic interference shielding [20–22].

Besides carbon, biochar contains some oxygen, hydrogen and inorganic elements (ash) [23], while bio-oil consists of water and complex mixture of oxygenated organic compounds like aldehydes, ketones, acids, alcohols, sugars, dehydrosugars and phenolic compounds [24–27], and the gas (non-condensable vapor) is composed of components like CO_2, CO, H_2, CH_4, and other light hydrocarbons (C_xH_y) [25,26,28,29].

Biochar production and application is a prominent climate change mitigation option, because biochar can sequester stable carbon and reduce greenhouse gas emissions from both atmosphere and soil [30–35], with the IPCC already recognizing it as a carbon dioxide removal (CDR) method necessary to achieve net zero CO_2 and GHG emissions both globally and nationally [36].

Livestock residues like bones and manures of different animals are being explored as the feedstock for production of biochar, bio-fuel and syngas, as these are massive sources of greenhouse gases (GHGs) emission [37,38]. In addition, rice husk is one of the most plentiful agricultural residues in Asian countries [39]. Furthermore, these biomass, such as bones, manures, bedding materials, wasted feeds, rice husk, rice straw, and other wastes, contain huge amounts of cellulose, hemicellulose, lignin, pectin and other organic materials [40,41]. So, pyrolysis of these biomass produces biochar which contains numerous pores, oxygen functional groups, and aromatic surfaces [42].

The advancements in pyrolysis research and decentralized biomass valorizations are constrained by limited access to affordable reactors. Most available reactors in the market are designed for either pilot-scale or industrial-scale applications, making them expensive, particularly in developing countries [43,44]. Dependence on imported parts makes component replacement and maintenance difficult and expensive as well [43]. Low-cost, laboratory-scale, locally fabricated, and open-access pyrolysis batch reactors remain understudied and scarce, particularly in developing countries, creating a structural barrier to biochar adoption where it's needed the most. Besides, existing studies on low-cost reactors are limited in scope. Previous designs focus on specific applications, such as, producing charcoal for domestic cooking and heating [45], enhancing feedstock mixture during pyrolysis for plastic waste conversion [46], or upgrading biofuel pallets suitable for biochar production [47]. But they often lack broader applicability. Recent work of Ibitoye et al., 2025 is one of the few efforts that focus on research and academic-based reactor design [43]. Although their reactor can collect solid, liquid, and gas; their work exhibits thermal gradient issues with limited control over internal heat distribution. Furthermore, their study does not quantify reactor fabrication cost or biochar operating energy cost, and reports only product yields (%) without assessing product quality through characterization techniques, such as, FTIR, XRD, and ICP-MS. More broadly, most reactor design-oriented studies do not incorporate detailed product quality assessments [48–50].

To address these gaps, this study designs and develops a pyrolysis reactor that offers an accessible alternative, suitable for laboratory-scale research, and small-scale decentralized rural applications in developing countries. The reactor model has been developed using SketchUp software and been fabricated in a local engineering workshop, demonstrating the feasibility of indigenous reactor construction using local materials. Besides the design, this study includes engineering performance evaluation and scientific validation, reporting functional groups, crystallinity, morphology and heavy metal concentrations of the products. The developed reactor has control over pyrolysis conditions (final temperature, residence time), making it process-oriented and experimentally rigorous. This study also quantifies both reactor fabrication and biochar operating energy cost.

Therefore, the primary objective of this study is to present the engineering design, local fabrication process, and economic feasibility of a low-cost pyrolysis reactor suitable for laboratory research and decentralized rural applications. The secondary objective aims to validate the reactor's capacity to produce structurally distinct, agronomically safe biochar across its operational temperature range, including biochar yield assessments from various biomass feedstocks at temperatures ranging from 450 °C to 700 °C, temperature-dependent structural evolution of biochar at 450 °C and 600 °C, and physicochemical characterization of the condensed liquid by-product. As a tertiary objective, the study also conducts a preliminary field assessment of short-term effects of biochar on growth and yield parameters of two high-yielding rice varieties, establishing baseline agronomic data for long-term evaluation.

Overall, the work facilitates the development of affordable and sustainable biomass conversion systems and decentralized waste valorization pathways relevant to circular economy practices in resource-constrained regions. Additionally, the work contributes to several United Nations Sustainable Development Goals (SDGs), including SDG 9 (industry, innovation, and infrastructure), SDG 12 (responsible consumption and production), and SDG 13 (climate action), with additional relevance to SDG 2 (zero hunger), SDG 7 (affordable and clean energy), SDG 11 (sustainable cities and communities), and SDG 15 (life on land).

2. Methodology and materials

Biochar was produced through slow pyrolysis process along with condensed liquid by-product in our designed reactor at different pyrolysis temperatures at the Physics Laboratory, Bangladesh Agricultural University (BAU), Mymensingh. The structural and physicochemical experiments were performed at Central Laboratory, BAU, Mymensingh, at Bangladesh Atomic Energy Commission (BAEC), Dhaka, and at Bangladesh Council of Scientific and Industrial Research (BCSIR), Dhaka. Besides, the short-term effects of biochar treatments on plant growth and yield parameters were experimented at the Soil Science Field Laboratory, BAU, Mymensingh.

2.1. Biomass feedstocks selection and preparation

Livestock wastes (poultry manure, bones) were collected from the Poultry Farm, BAU, whereas, rice husk and wood flakes were collected from nearby rice mill and saw mill of BAU, respectively. Thereafter, these raw materials were dried separately under direct sunlight for five days to attain minimum moisture content before pyrolysis. The final moisture content for each feedstock was <30%, however, specific amount was not recorded, introducing potential uncertainty in mass balance calculations, as residual moisture can influence yields of pyrolysis products [52]. Future work will incorporate standardized moisture determination method like ISO 18,134–2 to improve the accuracy of mass balance and yield estimation.

2.2. Design and construction of the pyrolysis reactor with working principles

The cylindrical pyrolysis reactor was designed and constructed for laboratory-scale research and small-scale rural applications, considering both theoretical principles and practical constraints. The design incorporated critical pyrolysis parameters, such as operating temperature, heating rate, and residence time, to optimize thermochemical conversion and biochar quality [23,53].

The physicochemical characteristics of raw materials were also considered, as they significantly influence the thermal decomposition behavior and biochar yield during pyrolysis process [54]. Taking all these into account, this SketchUp modeled reactor was fabricated at a local Engineering Workshop in Mymensingh.

Fig. 1(a) and Fig. 1(b) show the schematic diagram and 3D model of

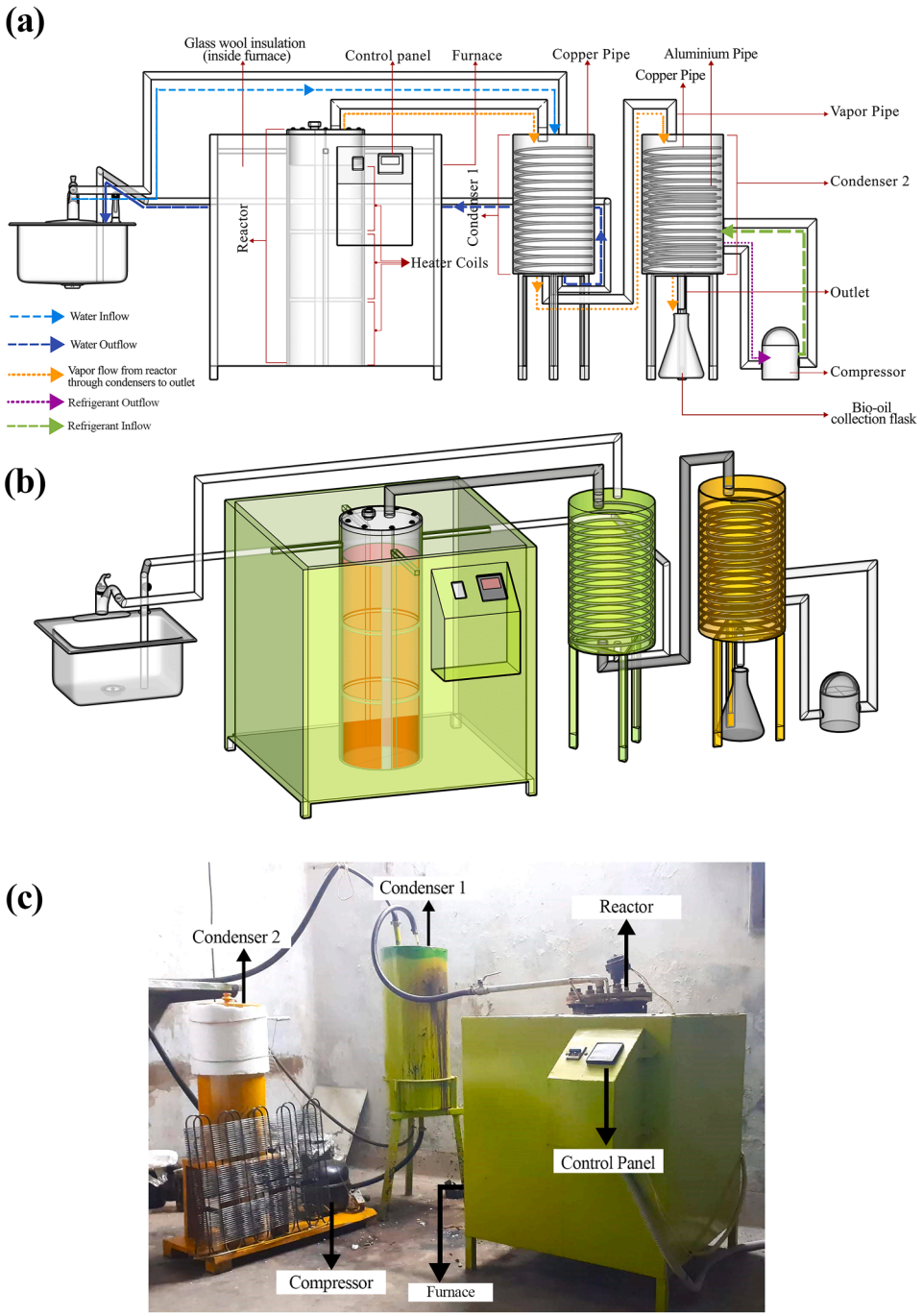

Fig. 1. The pyrolysis reactor system (a) Schematic diagram with working principles, (b) 3D Model with working principles, (c) Photograph of the fabricated reactor at Physics Lab, BAU.

the reactor system with its working principles, respectively, while Fig. 1 (c) shows the actual photograph of the constructed reactor system. Table 1 explains the specifications of the reactor system.

Pyrolysis of biomass was performed using the reactor unit consisting of a pyrolysis digestion chamber inside the furnace, three ceramic heating coils, two condensers, first one with spiral copper pipes, and second one with aluminum pipe, copper pipe, and a compressor, as shown in Fig. 1. The coils could provide controlled heating at a constant temperature up to 1000 °C. There was a vent at the top of the heating chamber, which was connected to the first condenser through a heat-proof plastic tube. Another heat-proof plastic tube went from first condenser to the second one. The condensers were cylindrical shaped chambers made of mild steel. The vapored gas exited the reactor and entered the 1st condenser through the plastic tube, where it flowed through the copper pipe. It then passed into the 2nd condenser through the second plastic tube, and flowed through the aluminum pipe, after which the resulting liquid and uncondensed gas exited from the bottom. The liquid was collected in a flask, while the gas was released without being collected.

The 1st condenser used water cooling, the condenser shell was filled with water like a reservoir, and a continuous inflow and outflow of water was maintained throughout the process. The 2nd condenser used refrigerated cooling controlled by a compressor, with R-134a (1,1,1,2-tetrafluoroethane, CH_2FCF_3 gas) serving as the cooling agent (refrigerant). In the second condenser, the R-134a (CH_2FCF_3) refrigerant flowed through the copper pipe, and continuous inflow and outflow of

Table 1
Reactor specifications.

Components	Specification	Value
Digestion chamber (Reactor)	Material	High carbon steel
	Height (ft)	2.5
	Outer diameter (in)	8.5
	Inner diameter (in)	7.5
	Wall thickness (in)	1
Heating coils	Material	3 ceramic coils
	Capacity (°C)	Up to 1000 °C
	Power (watt)	3000 W per coil × 3 coils
Heating rate	°C/min	3.75 (for 450 °C), 5 (for 600 °C), 5.83 (for 700 °C)
Residence time	Hour	1 (for all temperatures)
Isothermal Production rate	gm/min	6.67–21.5 (temperature and feedstock dependent)
Condenser-1	Material	Copper spiral pipe
	Material length (ft)	200
	Material diameter (in)	0.5
	Body material	Mild steel
Condenser-2	Cooling agent passage	Copper spiral pipe
	Vapor passage	Aluminum spiral pipe
	Cooling agent	R-134a (CH_2FCF_3 gas)
Cooling system	Condenser-1	Water cooling
	Condenser-2	compressor-driven refrigeration
Heat protector	Insulating material	Glass wool
Furnace	Material	Mild steel

refrigerant between the compressor and second condenser were maintained, while the gas coming from the 1st condenser flowed through the aluminum pipe.

High carbon steel was selected as the reactor construction material because it was more economical than stainless steel, and provided adequate structural strength, making it suitable for both laboratory-scale and small decentralized applications at lower cost. Standard ceramic heating coils were used due to their thermal stability, oxidation resistance, and thermal shock resistance [55,56].

The reactor had a controlled operational design capacity of 1000 °C, up to which, stable, repeatable, and safe thermochemical operations had been demonstrated. On the other hand, the experimentally validated operating window in the study was 450–700 °C, which was selected because literature suggests that under these conditions, slow pyrolysis biochar exhibits the optimal balance of yield, surface functionality, aromaticity, stability, pore structure, and agronomic safety for soil-amendment and carbon-sequestration applications [57–60].

2.3. Pyrolysis process of feedstocks and product recovery

The sun-dried poultry manure, bones, wood flakes, and rice husk were weighed (approximately 2000–3000 *g* per batch), tightly packed into the pyrolysis digestion chamber, and then, was placed in the reactor for heating. The reactor was operated at various fixed temperatures ranging from 450 °C to 700 °C. Temperature was raised from 0 °C to the targeted value in two hours, and then was kept in that temperature for one hour (residence time) for pyrolysis of different batches, with heating rate of 3.75–5.83 °C/min, and isothermal biochar production rate of 6.67–21.5 *g*/min, depending on operating temperatures and feedstock.

As the reactor temperature exceeded approximately 250 °C, pyrolysis vapors (volatile products) began to escape from the digestion chamber through the outlet in the lid and were directed into the condensers via the furnace vent. At the target temperature, volatiles continuously escaped from the digestion chamber and were subsequently condensed into liquid by-product in the condensation chambers, collected from the bottom of second condenser.

Oxygen-limited environment was achieved inside the digestion chamber by sealing and air-tightening the furnace lid, while glass wool was used as insulating material inside the furnace as heat protector. The continuous emission of pyrolysis volatiles from the digestion chamber further prevented air from diffusing in through the outlet in the lid. Initially, only one condenser was in the design. The second condenser was later included in the design to reduce loss.

The reaction (pyrolysis) time between the start and end of visible vapor release from the reactor was recorded, which was about 140 min. After completion of pyrolysis, the digestion chamber was removed from the furnace and was allowed to cool to room temperature, with the outlet sealed using a metal plug. The resulting black biochar solids in the digestion chamber and condensed liquid from bottom of second condenser were collected and stored at room temperature for further structural and physicochemical characterization. The products were weighed and yields were calculated from [61]:

$$Yield\ (\%) = (mass\ of\ product\ /\ initial\ dry\ feed\ mass) \times 100$$

$$Loss\ (\%) = 100 - (Biochar\% + Biooil\%)$$

The remaining fraction was reported as Loss (%), which might have included unrecovered condensable and non-condensable gases, and other system losses. It was reported as a mass-balance closure parameter. The present reactor configuration did not include a gas-capture or gas analysis unit. So, this fraction should not be interpreted as a direct measurement of syngas yield or gaseous product composition, which is a major design limitation subject to future improvements.

2.4. Characterization of biochar

Some experimental analyses were performed to assess structural, physical and chemical properties of the biochar samples produced from only poultry manure at 450 °C and 600 °C, such as, FTIR, XRD, SEM, and ICP-MS.

2.4.1. Fourier-transform infrared spectroscopy (FTIR) analysis

The FTIR spectra were recorded in transmission mode to identify functional groups in the biochar samples at the laboratory of BAEC, Dhaka. The spectra were collected over a wavenumber range of 4000 cm^{-1} to 400 cm^{-1} with a spectral resolution of 4 cm^{-1}. The analysis was carried out using a PERKINELMER L1600300 Spectrum TWO LiTa FT-IR Spectrometer.

2.4.2. X-ray diffraction (XRD) analysis

X-ray diffraction was employed to characterize the crystalline structure of biochar samples at the BCSIR laboratory, Dhaka, using a Rigaku SmartLab diffractometer. The samples were scanned in the diffraction angle (2θ) range of 10–80° with a scan rate of 1°/min.

2.4.3. Scanning electron microscope (SEM) observation

Scanning electron microscopy was conducted at the BCSIR laboratory, Dhaka, to examine the surface morphology and microstructure of the biochar samples. A Zeiss Evo 18 Electron Microscope was used with a resolution of 3 nm at an accelerating voltage of 30 kV in secondary electron (SE) mode, and <10 nm at 3 kV in high vacuum (HV) mode. The samples were analyzed over a magnification range of 2000x to 100,000x.

2.4.4. Inductively coupled plasma mass spectrometry (ICP-MS) analysis

Inductively Coupled Plasma Mass Spectrometry (ICP-MS) was used to determine the concentration of heavy metals in the biochar samples through ICP-MS machine at Central Laboratory, BAU. Prior to analysis, the biochar samples were digested using an appropriate acid digestion procedure and then, the digested solutions were analyzed to quantify elemental concentrations in ppm.

2.5. Characterization of the condensed liquid by-product

The condensed liquid produced as by-product from poultry manure at 450 °C and 600 °C was collected from the bottom of second condenser and was characterized through standard physicochemical analyses. Measured properties included color, density, kinematic viscosity, specific gravity, carbon residue, and gross calorific value, to evaluate the quality and fuel potential of the liquid.

The color was determined using the ASTM color scale, which ranges from 0 (no color) to 8 (dark or nearly black color, indicating presence of heavy organic compounds). The density and specific gravity were measured according to ASTM D1298 method. The kinematic viscosity was measured following ASTM D445 method. The carbon residue was measured using ASTM D189 to quantify the amount of carbonaceous material remaining after the removal of volatile components. Finally, the gross calorific value (also known as higher heating value) of the by-product was attempted using a Bomb Calorimeter. All these analyses were conducted at the BCSIR laboratory, Dhaka.

2.6. Effect of biochar treatments on plant growth and yield parameters

High yielding boro rice varieties, BRRI Dhan-88 and BRRI Dhan-89, were used to evaluate the effects of different biochar treatments on growth and yield parameters compared to normal condition (no biochar).

The experiment was conducted using a randomized complete block design (RCBD) with three replications to minimize field variability. Each block contained all treatments once in random order. A total of 30 plots were established, each plot measuring 2 m × 2 m, with 1 m spacing between replications and 0.50 m spacing between adjacent plots.

Five treatments (biochar levels) were applied: normal condition (no biochar application), bone biochar 0.75 and 1.75 (0.75 kg/plot and 1.75 kg/plot biochar application, respectively, produced at 700 °C), rice husk biochar 0.75 and 1.75 (0.75 kg/plot and 1.75 kg/plot biochar application, produced at 600 °C).

Growth and yield parameters considered at both milking and harvesting stages of plant were: Plant height (cm), shoot biomass (gm), root biomass (gm), total biomass (gm), grain yield (gm), and straw yield (gm). All the weights were sun-dried weight.

One-way ANOVA was used to assess the effects of biochar treatments on these parameters, and significant results ($p < 0.05$) were further analyzed using Tukey's HSD post-hoc test to determine pairwise differences among treatment means.

3. Results & discussions

3.1. Basic economic evaluation of constructed pyrolysis reactor

The constructed pyrolysis reactor is designed as a low-cost system for both laboratory-scale research and small-scale rural sustainability applications. The construction cost (in Table 2) and operating energy cost per batch (in Table 3) demonstrate its economic feasibility. The total construction cost of the reactor system is approximately 557.02 USD, indicating its affordability for decentralized biomass valorization and waste management applications. The heating coils may require replacements after pyrolyzing around 15–20 batches, with each batch containing 2–3 kg of biomass residues.

Table 2
Construction cost of the full reactor system. Used currency exchange rate (on April 1, 2026) was 1 USD=122.98 BDT.

Component	Specification	Amount (BDT/USD)
Reactor	High carbon steel	25,000/203.29
Heating coils	3 ceramic coils*2000 BDT	6000/48.79
Condenser-1	Mild steel with copper pipe	15,000/121.97
Condenser-2 and Compressor	Mild steel with copper and aluminum pipe	10,000/81.32
Heat protector	Glass wool	2500/20.33
Miscellaneous	labor, materials, parts, others	10,000/81.32
	Total (BDT/USD)	68,500/557.02

Table 3
Average operating energy cost of biochar per batch at 600 °C. Used currency exchange rate (on April 1, 2026) was 1 USD=122.98 BDT.

Parameters	Values (per batch)
Production capacity	1005 *g* (on average)
Production time	3 h
Raw material cost	-
Other cost	-
Consumed energy[a]	5.94 kWh
Power cost[b]	45 BDT (0.37 USD)

[a] Consumed energy= 1.98 kW × 3 h = 5.94 kWh.
[b] Estimated cost= 5.94 kWh × 7.55 BDT/kWh = 44.847 BDT.

The reactor operates with low energy requirements. For producing biochar at 600 °C through pyrolysis, temperature is increased to 600 °C in 2 h, and then is maintained at 600 °C for 1 hour. The system consumes 1.98 kW energy, resulting in a total energy consumption of 5.94 kWh per batch. The energy cost per batch is estimated at 45 BDT/0.37 USD and each batch produces 750gm-1260gm (1005gm on average) of biochar at 600 °C, depending on feedstock (except for wood flakes), while local market price of 1000gm of biochar in Bangladesh is in the range of 65–70 BDT (0.53–0.57 USD), indicating economic competitiveness at small-scale.

Electricity rate according to Bangladesh Power Development Board (BPDB) is 5.25 BDT/kWh for rural agricultural/poultry farms and 7.55 BDT/kWh for universities/educational/research institutions. In this paper, the rate used for cost calculation is 7.55 BDT (0.061 USD), meaning the operating energy cost may be lower in local rural households or farms.

Previously developed pilot-scale reactors costed as low as 0.394 USD/kg production [62], 0.581 USD/kg production [63], or 0.7 USD/kg production [64], while some ranges were around 0.528–1.051 USD/kg production [65], 0.611–1.061 USD/kg production [66], or 0.448–1.846 USD/kg production [67], compared to 0.37 USD/kg operating energy rate of this reactor. It should be noted that, as the primary objective of this study is academic research and rural sustainability, and not industrial-scale production or revenue generation, deeper techno-economic analyses like OPEX, CAPEX, or profitability were not incorporated.

3.2. Yield achieved through thermochemical conversion

Product yields shown in Table 4 demonstrate valorization of the biomass residues at different temperatures into value-added carbon material (biochar) and a potential energy-containing liquid by-product. For poultry manure, increasing temperature from 450 °C to 600 °C has reduced biochar yield and has increased bio-oil yield, indicating enhanced devolatilization and redistribution of carbon to condensable vapors at elevated temperature [38]. For wood flakes and rice husk, biochar yield has decreased substantially with increasing temperature, consistent with intensified volatile release. Losses should be interpreted as mass-balance closure.

Product yields for each pyrolysis condition in Table 4 are obtained from three independent experimental runs, and the reported values represent the mean of these three trials. In contrast, FTIR, XRD, SEM, and ICP-MS, along with by-product analyses are conducted on representative samples and are presented as single-trial results.

Previous studies have shown that around 45.68% and 37.9% yield can be produced from rice husk biochar at 450 °C and 600 °C, respectively [68], compared to 40% and 37.5% yield in this study. From various wood flakes, previous studies have produced around

Table 4
Production Analysis and Yield of Bio-char & Bio-oil.

Feedstock	Temp.	Amount (gm)	Bio-char (gm)	Bio-oil (gm)	Biochar yield (%)	Bio-oil yield (%)	Losses (%)
Poultry manure	450 °C	3000	1290	1080	43	36	21
	600 °C	3000	1260	1200	42	40	18
Wood flake	600 °C	2500	680	500	27.2	20	52.8
	700 °C	2700	400	600	14.8	22.22	62.98
Bones	700 °C	3000	1240	-	41.3	-	-
Rice husk	450 °C	2000	800	-	40	-	-
	600 °C	2000	750	-	37.5	-	-

30.9–33.8% and 29.5–32.1% yield of biochar at 600 °C and 700 °C, respectively [69], compared to comparatively lower yield of 27.2% and 14.8% in this study. From chicken bones, around 55% yield was produced in literature at 700 °C [70], compared to comparatively lower yield of 41.3% in this study. From poultry manure, various studies have produced around 40.6–48% and 39.8–43.2% yield of biochar at 450 °C and 600 °C, respectively [71–73], compared to 43% and 42% yield in this study. Except for biochar produced from wood flakes at 700 °C, all the yield values produced in this reactor were similar to other studies.

3.3. Temperature-dependent structural evolution of biochar

3.3.1. FTIR test for biochar

The FTIR spectra of Biochar produced from poultry manure at 450 °C and 600 °C are recorded under transmittance mode and are shown in Fig. 2(a) and Fig. 2(b), respectively, with measured peak values of FTIR analysis mentioned in Table 5. On the surface of the biochar, various organic functional groups including hydroxyls and carbonyls are identified. The sharp and broad peaks observed at 3443 cm^{-1} and at 3445 cm^{-1} correspond to the O—H stretching vibrations of hydroxyl groups (alcoholic and phenolic) for 450 °C and 600 °C, respectively [74,75]. The peaks at 2924 cm^{-1} and 2926 cm^{-1} for 450 °C and 600 °C, respectively, along with the peak at 2855 cm^{-1} for both temperatures suggest the presence of aliphatic C—H stretching vibrations of -CH_n groups in the biochar [76–78]. The peaks observed at 1633 cm^{-1} and at 1620 cm^{-1} correspond to the C = C group, while literature finds either aromatic C = C stretching [79] or C = O functional groups [80] for 450 °C and 600 °C, respectively. The peak observed at 1385 cm^{-1} is C = O stretching of carboxylic acid functional groups at both temperatures, while literature suggests it might be attributed to either deformed -CH_3 [81], C—O stretching [82] or O—H bending [83] vibrations of carboxylic and phenolic functional groups. The peaks observed around 1104 cm^{-1} and 1036 cm^{-1} are related to the C—O stretching vibration of oxygen containing functional groups on the biochar surface at 450 °C and 600 °C, respectively [84]. The transmittance peaks between 873–790 cm^{-1} and 875–777 cm^{-1} for biochar produced at 450 °C and at 600 °C, respectively, are associated with aromatic C—H bonded compounds present on the surface of investigated sample [85]. Specific spectral peaks (cm^{-1}) at both temperatures are shown in Table 5.

Table 5
Comparison data of FTIR peak analysis.

SL	Temp.	Unit	FTIR Spectrometry Results
01.	450 °C	cm^{-1}	3443, 2924, 2855, 1633, 1385, 1104, 873, 790, 618
02.	600 °C	cm^{-1}	3445, 2926, 2855, 1620, 1385, 1036, 875, 777, 588, 585, 478

3.3.2. XRD test of biochar

In Fig. 3(a), the XRD pattern of biochar produced at 450 °C shows a broad diffraction hump around 2θ ≈27–30°, indicating the predominance of amorphous carbon and silica [86]. Another peak near 2θ ≈40° is also observed, which may be associated with disordered carbon structures. With an increase in pyrolysis temperature to 600 °C, Fig. 3(b) shows comparatively sharper peaks appear near 2θ ≈27°, corresponding to the (002) plane of graphitic carbon, suggesting the development of more ordered carbon structures [80]. Additionally, even more intense and sharper peak near 2θ ≈40° can be attributed to the (100) plane of turbostratic carbon [87], along with weak reflections corresponding to crystalline SiO_2. The increased sharpness of peaks at 600 °C indicates enhanced carbonization and crystalline nature, along with structural ordering of the sample [75]. Overall, increasing pyrolysis temperature remove non-carbonaceous elements (O, H, N, S), leading to improved structural organization of biochar. Characteristics of biochar at both temperatures are summarized at Table 6.

3.3.3. SEM analysis of biochar

SEM analysis shown in Fig. 4 reveals that biochar particle sizes range 29.0–47.1 nm (Fig. 4b) with pore sizes of 1.31–2.06 μm (Fig. 4a) at 450 °C, while, particle sizes range 30.7–65.0 nm (Fig. 4d) with pore sizes of 2.01–5.45 μm (Fig. 4c) at 600 °C. So, the SEM figures qualitatively show that biochar produced at 600 °C exhibits rougher surfaces and larger visible pores than biochar produced at 450 °C, indicating greater apparent pore development at higher pyrolysis temperature [88].

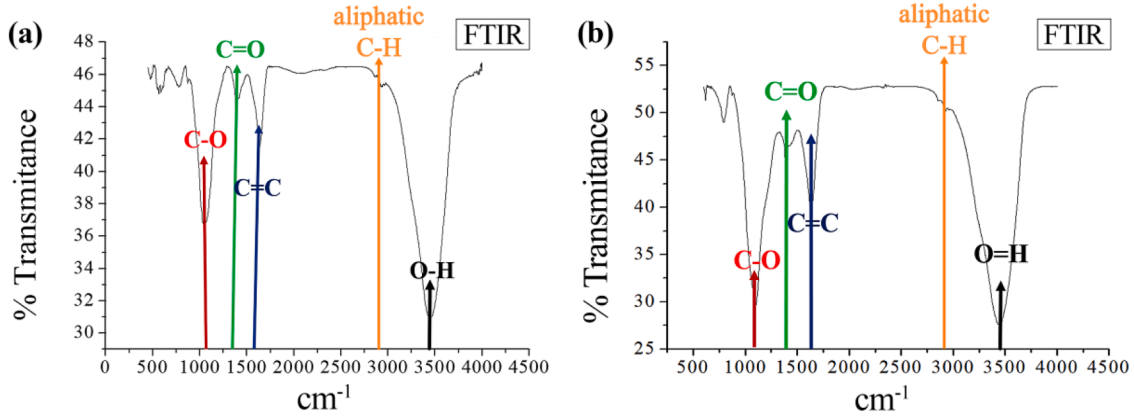

Fig. 2. FTIR peak positions under transmittance mode at (a) 450 °C and (b) 600 °C.

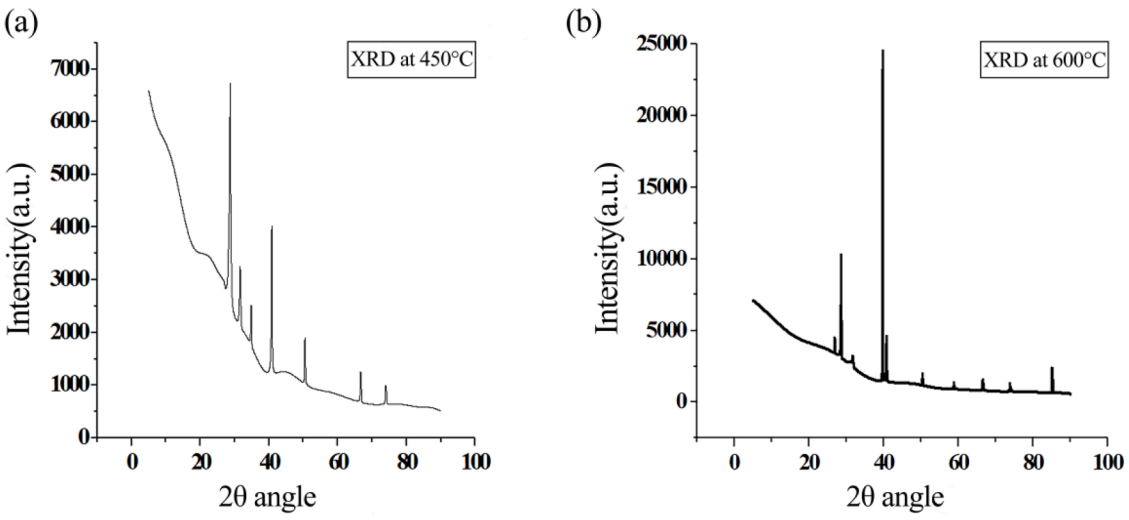

Fig. 3. XRD Peak positions in Biochar at (a) 450 °C and at (b) 600 °C.

Table 6
Summary characteristics of biochar samples from XRD.

Feature	Biochar at 450 °C	Biochar at 600 °C
Carbon Structure	Highly disordered	More ordered
Silica	Most amorphous	Partially crystalline
Peak width	Broad	Shaper
Graphitization	Very low	Moderate

According to International Union of Pure and Applied Chemistry (IUPAC), pores are classified as micropore (diameter < 2 nm), mesopore (2 nm < diameter < 50 nm), and macropore (diameter > 50 nm) [89]. Based on this IUPAC classification, observed pores fall within the macropore range. These morphological differences are consistent with increased release of volatile organic matters from biomass during the pyrolysis process [90].

However, no BET or other adsorption-based surface area analysis has been conducted in this study, and SEM observations alone cannot be

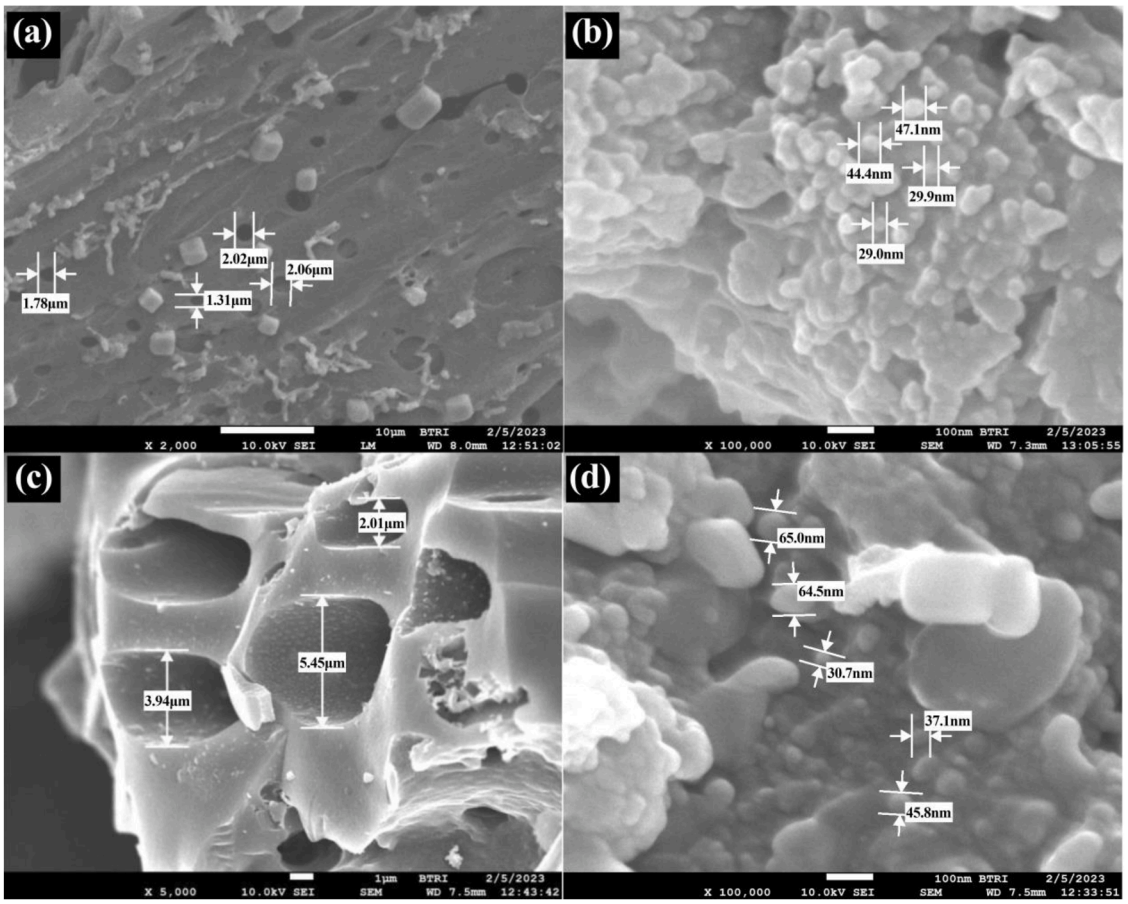

Fig. 4. SEM Images of Biochar samples. (a) Pore sizes at 450 °C, (b) Particle sizes at 450 °C, (c) Pore sizes at 600 °C, (d) Particle sizes at 600 °C.

interpreted as direct evidence of increased specific surface area [91,92]. Therefore, the SEM results are discussed here only in terms of qualitative surface morphology and pore structure, rather than quantitative claims.

As, studies about immobilizing lac-case on biochar have been seldom reported [93], different biochar may present different chemical or physical properties related to different raw materials or production conditions in order to support enzyme immobilization [76]. So, our findings may influence the utilization of biochar for enzyme immobilization.

3.3.4. ICP-MS test of biochar

Heavy metals, such as Fe, Mn, Zn, Cu, Cr, Ni, Pb, Co, Se, and Cd are quantified using ICP-MS analysis and their concentrations are mentioned in Table 7. Increasing pyrolysis temperature from 450 °C to 600 °C results in decreased concentration for most heavy metal elements, although Ni and Cd show slight increase. Overall, total concentration of these measured heavy metals decrease with higher pyrolysis temperature, contradicting Kujawska et al., 2024, which may be attributed to elemental redistribution, volatilization of certain components, and mass loss during pyrolysis [94,95]. Concentration of these elements at both temperatures are way below the maximum allowable limits reported by International Biochar Initiative (IBI) in 2015, meaning each biochar satisfies threshold values for total heavy metal content.

However, only total concentrations of the elements are measured and compared in this study, limiting direct indication of speciation, leachability, mobility, or bioavailability, warranting further investigation [96]. Therefore, no definitive conclusion can be drawn regarding improved chemical stability, stronger immobilization of toxic metals, or reduced environmental and ecological risk at higher pyrolysis temperature, which was found by Wang et al., 2019 [97]. Further leaching and speciation analyses are needed to directly assess these possibilities.

3.4. Physicochemical properties of condensed by-product (Bio-oil)

Table 8 presents the physicochemical properties of the condensed liquid by-product obtained at 450 °C and 600 °C with appropriate methods. The liquid produced at 450 °C exhibited higher density, viscosity, specific gravity, and carbon residue than the liquid produced at 600 °C.

Both samples exhibit a dark color (ASTM scale > 8.0), indicating the potential presence of a wide range of complex organic compounds including sugars, esters, ethers, carboxylic acids, alcohols, aldehydes, ketones and phenols [98–100]. The kinematic viscosity values are as low as 0.96 and 0.94 cSt (at 40 °C) for 450 °C and 600 °C, respectively, suggesting the recovered liquid fractions to be dominated by aqueous components rather than bio-oil because viscosity of bio-oil produced from poultry manures in some previous literature is as high as 130–9050 cSt, independent of analysis methods [101,102]. This observation is further supported by the values of densities (1.0307 and 1.0240 g/cm^3 for 450 °C and 600 °C, respectively) and specific gravities (1.0321 and 1.0254 for 450 °C and 600 °C, respectively), which are close to that of water. Literature suggests that density of organic-rich bio-oil produced from poultry manure can be around 1.14–1.18 g/cm^3 [101,102] and specific gravity can be around 1.18 [102]. Carbon residue (w/w%) of the by-product is 1.043 at 450 °C, which significantly reduces to 0.51 at 600 °C, improving fuel property of by-product, as low carbon residue fuel is recommended for sustainability [103]. Higher presence of carbon residue indicates poorer fuel quality and its amount in bio-oil can be in range of 0.28–0.57 [104]. The gross calorific value cannot be determined for either sample as the water content is very high (~80%), whereas, bio-oil produced from poultry manure can replicate calorific value from 23.3 MJ/Kg to as high as 40.32 MJ/Kg [101,102,105].

Decreasing viscosity, density, specific gravity and carbon residue with increasing pyrolysis temperature indicates enhanced thermal cracking and the formation of lighter, more volatile compounds [106–109]. The results suggest that the liquid products obtained primarily consist of water-rich condensates with limited fuel potential, highlighting the need for process optimization or upgrading techniques to improve bio-oil quality.

Table 7
Heavy metal testing report with digestion through ICP-MS machine.

Element Name	Symbol (Z)	At 450 °C (ppm)	At 600 °C (ppm)	Maximum allowable range by IBI (ppm, dry wt.)
Chromium	Cr (24)	29.75	20.95	93–1200
Manganese	Mn (25)	223.25	168.75	-
Iron	Fe (26)	2625	1032.5	-
Cobalt	Co (27)	0.9175	0.725	34–100
Nickel	Ni (28)	10.9	21.5	47–420
Copper	Cu (29)	31	20.4	143–6000
Zinc	Zn (30)	168.5	91.25	416–7400
Selenium	Se (34)	0.575	0.4425	2–200
Cadmium	Cd (48)	0.1445	0.1555	1.4–39
Lead	Pb (82)	2.925	0.96	121–300

Table 8
Physicochemical Properties of the liquid by-product.

Test	Method/ Instrument	At 450 °C	At 600 °C
Color	Colorimeter	ASTM scale > 8.0, black	ASTM scale > 8.0, black
Density (gm/cm^3) at 15 °C	ASTM D1298	1.0307	1.0240
Viscosity (cSt) at 40 °C	ASTM D445	0.96	0.94
Specific Gravity	ASTM D1298	1.0321	1.0254
Carbon Residue, % (w/w)	ASTM D189	1.043	0.51
Gross Calorific Value (MJ/Kg)	Bomb Calorimeter	Could not be determined for either sample due to high water content (~80%)	

3.5. Mechanistic basis for temperature-dependent product evolution

The temperature-dependent changes of products in this study in terms of yield, surface chemistry, porosity, and condensed liquid composition are dictated by five combined mechanisms, intra-particle heat transfer, primary volatile release, secondary vapor-phase cracking, carbonization, and structural rearrangement [110,111]. Each mechanism responds differently to pyrolysis temperature, and controls the thermochemical conversion of biomass altogether [110,112]. As non-condensable gas is not recovered in this study, the temperature-dependent changes are interpreted as overall shift in product partitioning rather than increased gas yield.

At the particle-scale, intra-particle heat transfer controls how rapidly the reaction front penetrates the biomass interior. Conductive heating from the coils creates internal temperature gradients, expanding residence time distribution of devolatilizing biomass and shifting local kinetics relative to isothermal prediction [110,111]. CFD modeling shows these gradients steepen with set-point temperature, accelerating volatile escape and reducing the time available for tar re-deposition [110]. Comparable behavior has also been documented at the reactor scale in tubular thermochemical systems, where radial temperature gradients depend on heating mode and affect thermochemical conversion uniformity [111]. These mechanisms collectively explain the systematic biochar-yield decrease from 450 °C to 600 °C across all four feedstocks (Table 4), with poultry manure showing larger condensed fraction and wood flakes showing larger unrecovered fraction.

Primary volatile release occurs through dehydration, decarboxylation, decarbonylation, and depolymerization of cellulose, hemicellulose, lignin, with associated protein, lipid, and mineral fractions of poultry manure and bones [112]. Cellulose and hemicellulose depolymerize in the 200–400 °C range and release levoglucosan,

anhydrosugars, furans, and light oxygenates, while lignin contributes to phenolic monomers in the range of 200–600 °C [112]. The progressive attenuation of FTIR bands for O—H stretching, aliphatic C—H, C = C groups, C—O groups, and aromatic C—H between 450 °C and 600 °C is the spectroscopic signature of this stepwise functional-group removal shown in Fig. 2 and Table 5.

As primary volatiles traverse the hot zone inside reactor, they undergo secondary vapor-phase cracking. Large oxygenates are converted into CO, CO_2, H_2, CH_4, water, and light hydrocarbons, while reactive intermediates partially repolymerize into secondary char and aromatic tar [110,112]. Cracking intensifies with temperature and vapor residence time, so the condensers capture the even lighter, water-rich fraction at higher temperature, mirrored by the reduced density, viscosity, specific gravity, and carbon residue at 600 °C (Table 8) and explaining the predominantly aqueous by-product noted in Section 3.4.

Carbonization and structural rearrangement function in parallel. Fixed-carbon enrichment is accompanied by aromatic ring condensation, polyaromatic growth, and sp^3 to sp^2 aromatic carbon conversion. The sharpening (002) and (100) reflections near $2\theta \approx 27^\circ$ and $2\theta \approx 40^\circ$ at 600 °C (Fig. 3) confirm coalescence of the amorphous matrix into turbostratic carbon [112,113]. The same volatile escape reshapes morphology. SEM-observed pore and particle enlargement at 600 °C (Fig. 4) arises as vapor fractions widen channels and open new macropores [113]. A slight decrease in heavy metal concentration at 600 °C (Table 7) indicates some volatilization and transfer into stable mineral forms as the matrix undergoes sintering.

3.6. Effects of biochar treatments on plant growth and yield parameters

Results of one-way ANOVA are presented in Table 9 to assess the effects of biochar treatments on plant growth and yield parameters. Only shoot biomass and total biomass at milking stage for BRRI Dhan-88 show significant effects ($p < 0.05$). These two parameters are further analyzed using Tukey's HSD post-hoc test to determine pairwise differences among treatment means and the results are shown in Fig. 5(b) and 5(f). Fig. 5(a-i) illustrates the numerical responses of different biochar treatments for both rice varieties, while Figs. 5(b) and 5(f) include Tukey letters indicating pairwise impact.

Overall, biochar produces stronger responses at the milking stage than at the harvesting stage, and the response is variety-dependent, with BRRI dhan-88 showing greater physiological responsiveness than BRRI dhan-89.

In Fig. 5(b) and 5(f), for BRRI dhan-88 at the milking stage, both shoot biomass and total biomass show significant response. One-way ANOVA is significant ($p = 0.005$), while Tukey's test shows that the strongest numerical response is under Rice Husk Biochar 1.75, followed by Bone Biochar 0.75. Also, strong numerical response is found under Rice Husk Biochar 1.75 compared to Rice Husk Biochar 0.75, suggesting a dose-dependent effect for rice husk biochar. This suggests that, in BRRI dhan-88, biochar stimulated response is not linear across all treatments and the effect depends on both source and rate. In contrast, BRRI dhan-89 shows no significant treatment effect for these parameters.

Table 9
One-way ANOVA showing effect of biochar treatments on growth and yield parameters of BRRI Dhan-88 and BRRI Dhan-89 (at 95% confidence level).

Variety	Growth Stage	Parameters	df	F	p
BRRI Dhan-88	Milking	Plant height	(4, 10)	.345	.842
		Shoot biomass	(4, 10)	7.355	.005*
		Root biomass	(4, 10)	.716	.600
		Total biomass	(4, 10)	7.244	.005*
	Harvesting	Shoot biomass	(4, 10)	.390	.811
		Root biomass	(4, 10)	.554	.701
		Total biomass	(4, 10)	.353	.836
		Grain Yield	(4, 10)	.770	.569
		Straw Yield	(4, 10)	.380	.818
BRRI Dhan-89	Milking	Plant height	(4, 10)	.830	.536
		Shoot biomass	(4, 10)	.070	.990
		Root biomass	(4, 10)	.314	.862
		Total biomass	(4, 10)	.078	.987
	Harvesting	Shoot biomass	(4, 10)	1.634	.241
		Root biomass	(4, 10)	.473	.755
		Total biomass	(4, 10)	.078	.987
		Grain Yield	(4, 10)	1.493	.276
		Straw Yield	(4, 10)	.342	.844

* Significant at $p < 0.05$.

Previous studies have reported mixed results regarding biochar application. Some studies have shown that sole application of biochar does not promote rice growth and yield parameters [114]. In contrast, other studies report increases in plant height, straw yield, grain yield, shoot biomass, root biomass, and total biomass with biochar application even without fertilizer [115,116]. Additionally, increased plant height and grain yield with biochar application combined with N fertilizer has also been observed [117]. Many studies also suggest that the effects of biochar are more pronounced in the long term, where all six growth and yield parameters improve over time, with biochar application without fertilizer [118] as well as combined with fertilizer [119–121]. So, the non-significant ANOVA and Tukey results observed in this study may be attributed to factors such as small sample size, short experimental duration, relatively low biochar application rates, and environmental variability, which may have limited the detectability of treatment effects.

Short-term single-season application of biochar at the tested rates do not produce statistically significant effects on most growth and yield parameters, indicating the need for multi-season biochar trials. These results establish baseline data for longer-term agronomic evaluations.

3.7. Comparison of research approach in this study with recent similar literature

Table 10 compares the main approach and results of present study with other recent similar low-cost, laboratory-scale, pilot-scale, mobile, solar, and locally fabricated pyrolysis reactor design studies. The closest direct comparator is the reactor of [43], which operates at similar feedstock loading (1 kg per batch) and within the same low-temperature window, but reports neither a quantified basic economic indicator nor full structural characterization of the resulting biochar. Pilot-scale and kiln-scale studies [49,122] achieve substantially higher absolute throughput (11–200 kg per batch up to 5 tons per batch) but at significantly higher capital outlay. For example, USD 18,458 total capital investment for the [62] pool reactor, and are oriented toward bio-adsorbent or commercial char. Solar [48] and earth kiln replacement [123,124] designs target different deployment functions. Across the full set, the present reactor delivers one of the lowest construction costs among electrically heated laboratory-scale comparators (USD 557 construction cost; USD 0.37 per kg biochar operating energy cost) and is differentiated by combining multi-feedstock validation (poultry manure, bones, rice husk, wood flakes), liquid by-product recovery, and full FTIR/XRD/SEM/ICP-MS structural characterization within a single study, a combination not jointly reported in any of the comparators surveyed.

4. Limitations of the present study

Although the developed pyrolysis reactor has showed promising performances regarding fabrication cost, operating energy cost, and biochar characterization, several important limitations of the study should be acknowledged for future improvements.

The biomass feedstocks are sun-dried for five days before pyrolysis, rather than following standardized methods, such as, ISO 18134–2. Although the final moisture content is <30%, exact values are not recorded. Feedstock moisture directly influences devolatilization behavior, product distribution, and condensed liquid composition. So, this omission introduces potential uncertainty into mass-balance

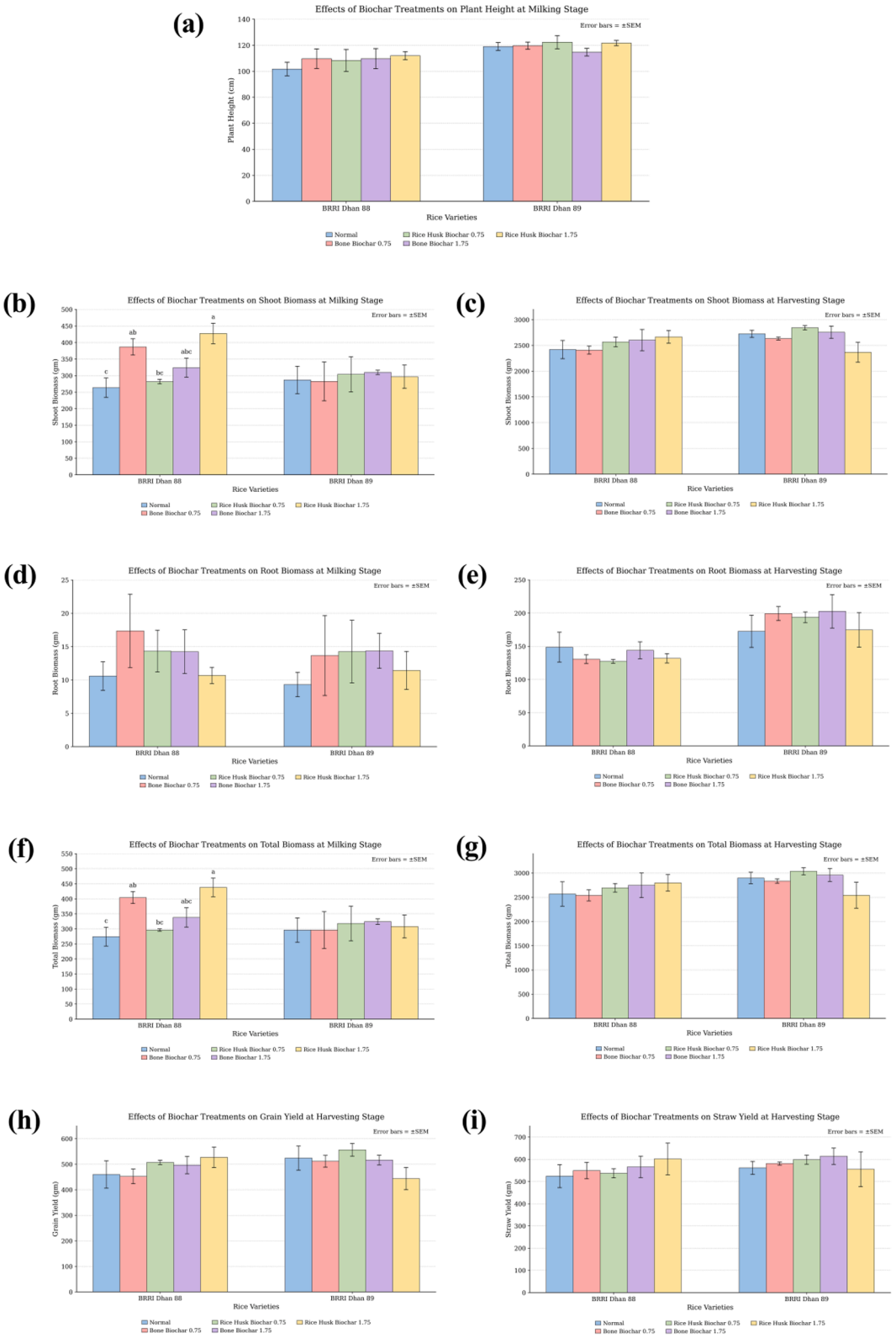

Fig. 5. Effects of different biochar treatments on (a) plant height at milking stage, (b) shoot biomass at milking stage, (c) shoot biomass at harvesting stage, (d) root biomass at milking stage, (e) root biomass at harvesting stage, (f) total biomass at milking stage, (g) total biomass at harvesting stage, (h) grain yield at harvesting stage, and (i) straw yield at harvesting stage.

closure, limiting strict comparison of product yields among feedstocks and temperatures.

The present reactor design does not include a syngas capturing unit. So, non-condensable gases are not directly quantified and characterized. The reported Loss (%) should be interpreted only as unquantified residual fraction rather than direct measurement of syngas yield. As a result, the study provides direct evaluation of the solid product (biochar) and condensed liquid fraction, not a complete characterization of all

Table 10
Comparison of the main approach of present study with other similar low-cost, laboratory-scale, pilot-scale, or locally fabricated pyrolysis reactor design studies.

Study	Main approach	Feedstocks	Scale and Temperature	Key Results (Yields)	Economic Indicator	Characterization Scope	Strengths	Limitations
This study	Electrically heated, laboratory-scale, low-cost, slow-pyrolysis batch reactor; Reactor performance evaluation by biochar yield at 450–700 °C and temperature-dependent structural evolution of biochar at 450 °C and 600 °C; Basic economic evaluation of the reactor.	Poultry manure, bones, rice husk, and wood flakes; 2–3 kg feedstock per batch.	Laboratory-scale batch reactor; Validation window: 450–700 °C; Operational design capacity: 1000 °C.	Biochar yields: 14.8–43 wt.% (feedstock and temperature dependent); Average biochar output: 1.005 kg per batch at 600 °C; Condensed liquid predominantly aqueous.	Reactor construction cost: USD 557.02; operating energy cost: USD 0.37 per kg biochar.	FTIR, XRD, SEM, ICP-MS; Condensate physicochemical analysis; Small-scale agronomic experiment.	Lowest construction cost among electrically-heated lab comparators; multi-feedstock validation; Condensate recovery; Combined FTIR, XRD, SEM, ICP-MS in one study; Locally fabricated.	No direct gas capture or quantification; Final feedstock moisture not specifically measured (ISO 18,134–2 recommended).
[122]	Dual-chamber batch pyrolizer with concentric cylinders and syngas recirculation; Performance evaluation of reactor through temperature profiles, energy balance, syngas production, and physicochemical characteristics of biochar.	Rice husk; about 11 kg feedstock per batch; 28 kg wood as fuel per batch.	Pilot-scale dual-chamber kiln; Operating range: 380–1000 °C.	Biochar yield: 42.37–49.28%; Production rate: 1.8 ± 0.2 kg h^{-1}; Syngas HHV: 23.3 ± 2.3 MJ m^{-3}; Specific surface area: 182 m^2 g^{-1}; Heat losses: 74.41–77.98%.	No economic assessment reported	BET surface area; Energy/mass balance; Syngas composition.	Low-complexity design with syngas reuse; Useful benchmark for small-scale decentralized operation.	Single-feedstock design (rice husk only); Liquid by-product not extracted; No economic assessment; High heat loss due to lack of insulation.
[43]	Portable, low-cost, laboratory-scale, batch pyrolysis reactor; Designed for university teaching and research; Char, oil, and syngas yields at three temperatures.	Rice husk and corncob; 1 kg feedstock per batch.	Laboratory-scale (1 kg); Tested at 450, 500, and 550 °C; Reactor maximum design: 1000 °C; Heater rating: 2.4 kW.	Yields: biochar 43.93–49.26%, oil 21.14–29.22%, syngas 25.63–32.01% (feedstock dependent); Higher temperature increased oil and syngas, reduced char.	Construction cost or Production cost not reported; Qualitative claim of "40–60% lower capital cost" compared to imported reactors.	Proximate, ultimate, sieve, and calorific (both rice husk and corncob); Yields of all three pyrolysis fractions.	Closest laboratory-scale comparator in recent years; Captures all three product fractions (char, oil, syngas); Locally fabricated.	No quantified economic assessment; Narrower spectroscopic or structural characterization than present study; Two feedstocks only.
[62]	Self-sustained, pilot-scale, pool-type carbonization reactor; Bio-adsorbent production for landfill leachate treatment; Comprehensive techno-economic assessment.	Woodchips; 3–5 tons feedstock per 7-day batch.	Pilot-scale pool reactor; Operating range: 300–700 °C; Heating rate: 5–7 °C per min; Annual capacity: 48 tons.	Biochar yield: 1 ton per batch (20 wt.%); BET surface area increased from 0.91 to 232.1 m^2 g^{-1} after pyrolysis; Average pore size reduced from 324.1 to 15.4 nm.	Plant cost: USD 12,678.78; Total capital investment (TCI): USD 18,458; Production cost: USD 394 per ton (USD 0.394 per kg); NPV: USD 36,905; IRR 94.6%; ROR 92.5% (10-year); Annual capacity 48 tons.	BET surface area; Pore size analysis; Adsorption performance (COD, TKN, NH_3-N).	Strong scale-up economics; Self-sustained operation; Decentralized deployment.	Substantially higher capital investment than present study; Oriented toward bio-adsorbent rather than agronomic use; No multi-feedstock validation.
[124]	Fixed-bed updraft reactor with condenser and separator; RSM-based residence time optimization at constant average temperature; Comparison with traditional Ethiopian earth-kiln method.	Eucalyptus; 22 kg feedstock per batch and 8 kg char per batch.	Pilot-scale (22 kg); Average pyrolysis temp: 415 °C; Residence times tested: 150–220 min.	Optimum char yield: 32.39% at 188.88 min; Maximum selectivity 72.02% at 161.69 min; Efficiency improved 24.17% compared to earth kiln method; Production time reduced by 150 min; CO and PM emissions reduced by 60.2% and 51.8%; Char HHV improved by 3 MJ kg^{-1} over traditional method.	No economic assessment reported.	Proximate and ultimate analysis (feedstock and char); Burning rate, time-to-boil, time-to-burn; Emissions (CO, PM, IAP measurements).	Condenser-equipped design; Statistical (RSM) optimization; Lower emissions than traditional kilns.	Single feedstock; No economic evaluation; No FTIR, XRD, SEM structural assessment of char.
[123]	Locally fabricated, low-cost, vertical pilot retort kiln;	Rice husk and corn cobs.	Pilot-scale kiln; Average Temp for EHT: 326.43	Higher biochar yield in EHT mode (37.23%) than IHT	Cost minimization stated qualitatively	Pyrolysis temperature profile; CEC, mineral	Dual-mode operation (IHT and EHT); Locally	Lower temperature range than present study; Liquid and gas

(continued on next page)

Table 10 (*continued*)

Study	Main approach	Feedstocks	Scale and Temperature	Key Results (Yields)	Economic Indicator	Characterization Scope	Strengths	Limitations
	Operates as top-lit updraft (IHT) or as dual-chamber (EHT); Performance evaluation of the kiln through biochar yield and physicochemical properties.		°C and for IHT: 423.72 °C.	mode (31.40%); Reduced pyrolysis duration in IHT mode; Higher organic C, P, and mineral contents in biochar from IHT mode; Biochar met basic EBC and IBI criteria.	(locally collected materials); No quantified economic indicator.	content, organic C, P; Particle size, density, water-holding.	constructed from recycled materials; Direct comparison of heat-transfer modes.	by-products not recovered or quantified; No techno-economic evaluation; No FTIR, XRD, SEM.
[48]	Theoretical design and evaluation of a small-scale solar-powered pyrolysis reactor (SPEAR); Cassegrain optics parabolic dish and manual tracking; Financial assessment under three carbon-credit scenarios.	Modeled agricultural and forestry wastes; Rice husk, sugarcane bagasse, corn straw, timber residue, eucalyptus residue; 5 kg biochar per unit per day.	Decentralized rural community scale; 200 L drum reactor; Achievable temp up to 750 K (≈ 477 °C); Reactor sizing: 7.5 kW.	Modeled char yield: 20–34 wt.% depending on feedstock; Optical efficiency up to 72% at 1.5° tracking error; Thermal efficiency > 70% across operating range; Electricity capacity: up to 240 W (5 TE units in series).	Modeled total capital cost: USD 1237; Positive NPV in nearly all scenarios; Order of magnitude lower than other reported solar-pyrolysis designs.	Optical (Monte-Carlo ray tracing); Thermal (heat-transfer model); Financial (NPV under three scenarios).	Integrates solar energy with biomass pyrolysis; Strong decentralized low-cost rationale; Co-produces biochar and electricity.	Theoretical study, no experimental validation; Product properties and condensate handling not measured; Lower achievable temperatures (477 °C) than present study.
[49]	Sustainable mobile biochar kiln with syngas recirculation; Process optimization via RSM with Central Composite Design (CCD); Physicochemical characterization of biochar.	Soybean straw; 200 kg feedstock per batch; Firewood used as heating fuel.	Pilot/farm scale mobile kiln; Design temp range: 450–650 °C; Steady-state center Temp > 500 °C.	Average biochar yield: 29.43 ± 1.42%; Energy conversion efficiency: 47.02%; Overall kiln efficiency 41.03%; Minimal fuel-to-biochar ratio 0.19 ± 0.02.	Payback period: 4.02 months; Benefit-cost (B/C) ratio and IRR optimized via RSM.	Proximate and elemental analysis; TGA; SEM/TEM.	Statistical optimization; Syngas integration; Strong fuel-use and economic metrics.	Less suited as a laboratory-scale comparator; Continuous firewood requirement alongside syngas; Heat loss during peak syngas production.

three principal pyrolysis products, which is a major limitation and scope for future improvements.

The SEM analysis is used to assess qualitative surface morphology and apparent pore development, and no BET or other direct surface-area analysis has been performed to quantify specific surface area. Similarly, the ICP-MS results represent total elemental concentrations only and do not directly indicate speciation, leachability, mobility, or bioavailability, limiting conclusion for metal immobilization behavior or environmental and ecological risk reduction.

The agronomic evaluation should be regarded as preliminary and short-term, involving limited treatment combinations. The results provide baseline observations rather than definitive agronomic validation.

In addition, the economic assessment is limited to fabrication cost and batch-wise operating energy cost. Broader techno-economic indicators such as CAPEX, OPEX, and profitability are beyond the scope of this work as the goal of this design is not industrial-scale production or revenue generation.

Future studies should therefore incorporate standardized feedstock moisture determination, gas collection and composition analysis, quantitative surface area measurement, leaching or speciation tests, longer-term field validation, and expanded techno-economic assessment.

5. Conclusion

This study establishes the engineering feasibility, economic viability, and analytical performance of a low-cost, locally fabricated, laboratory-scale, slow-pyrolysis batch reactor designed for decentralized biomass valorization in developing regions. With a construction cost of USD 557.02 and average operating energy cost of USD 0.37 per kg biochar, the reactor can compete favorably with substantially larger pilot-scale and kiln-based systems while offering controlled operation up to 1000 °C with a validated 450–700 °C window for poultry manure, bones, rice husk, and wood flakes.

A clear temperature-dependent structural transition is observed in poultry manure biochar between 450 °C and 600 °C, oxygen-containing functional groups attenuate (from FTIR), the carbon matrix evolves from a predominantly amorphous to turbostratic configuration (from XRD), apparent pore development increases (qualitative assessment from SEM), and total heavy metal concentrations decrease while remaining well below International Biochar Initiative threshold values for both temperatures (from ICP-MS). These findings link pyrolysis temperature to functional, structural, and agronomic safety outcomes, supporting feedstock and temperature-specific selection for soil amendment, carbon sequestration, or environmental remediation applications. The condensed liquid by-product is predominantly aqueous, and short-term agronomic responses are largely non-significant, underscoring the need for liquid-phase upgrading and longer-term field validation.

Key limitations include the absence of direct gas capture and quantification, and the absence of BET surface area, leaching, and metal speciation analyses. Future work will incorporate standardized feedstock moisture determination (ISO 18134–2), gas-phase composition analysis, BET adsorption-based surface-area measurement, leaching and speciation studies, multi-season agronomic trials, and broader techno-economic indicators (CAPEX, OPEX, profitability). Overall, the developed reactor offers an affordable, reproducible pathway for biomass-residue valorization aligned with United Nations Sustainable Development Goals 9, 12, and 13, with additional relevance to SDGs 2, 7, 11, and 15.

Funding information and acknowledgement

We acknowledge Ministry of Education, Government of People's Republic of Bangladesh for financing this Project (Project No: SD 20211555). Acknowledgement with thanks to Bangladesh Agricultural University Research System (BAURES) for providing technical support to run the project.

CRediT authorship contribution statement

Ishraque Mashiat: Visualization, Software, Investigation. **Alif Al Arefin Prodhan:** Writing – review & editing, Validation, Formal analysis. **Md. Mahbub Alam:** Methodology, Investigation, Formal analysis. **Md. Mukhlesur Rahman:** Supervision, Resources, Conceptualization. **Md. Khairul Hassan Bhuiyan:** Writing – original draft, Supervision, Resources, Project administration, Methodology, Investigation, Funding acquisition, Formal analysis, Data curation, Conceptualization. **Md. Kamrul Hasan Fakir:** Resources, Investigation.

Declaration of competing interest

The authors declare that they have no known competing financial interests or personal relationships that could have appeared to influence the work reported in this paper.

Data availability

Data will be made available on request.

References

[1] R. Eamrat, T. Pussayanavin, T. Kamei, K. Fakkaew, Physicochemical characterization and potential application of biochar produced from carbonization of chicken manure and biomass wastes, Int. J. Environ. Res. 20 (1) (2026) 21, https://doi.org/10.1007/s41742-025-00987-1.

[2] L. Li, et al., Relating bacterial dynamics and functions to greenhouse gas and odor emissions during facultative heap composting of four kinds of livestock manure, J. Environ. Manage. 345 (2023) 118589, https://doi.org/10.1016/j.jenvman.2023.118589.

[3] N. Rayne, L. Aula, Livestock manure and the impacts on soil health: a review, Soil Syst. 4 (4) (2020) 64, https://doi.org/10.3390/soilsystems4040064.

[4] F. Ronsse, R.W. Nachenius, W. Prins, Chapter 11 - carbonization of biomass, in: A. Pandey, T. Bhaskar, M. Stöcker, R.K. Sukumaran (Eds.), Recent Advances in Thermo-Chemical Conversion of Biomass, Elsevier, Boston, 2015, pp. 293–324, https://doi.org/10.1016/B978-0-444-63289-0.00011-9.

[5] A.K. Sakhiya, A. Anand, P. Kaushal, Production, activation, and applications of biochar in recent times, Biochar 2 (3) (2020) 253–285, https://doi.org/10.1007/s42773-020-00047-1.

[6] A. Budai, et al., Biochar carbon stability test method: an assessment of methods to determine biochar carbon stability, Int. Biochar Initiat. 1 (2013) 1–20.

[7] J.A. Ippolito, D.A. Laird, W.J. Busscher, Environmental benefits of biochar, J. Environ. Qual. 41 (4) (2012) 967–972, https://doi.org/10.2134/jeq2012.0151.

[8] S. Papari, K. Hawboldt, A review on the pyrolysis of woody biomass to bio-oil: focus on kinetic models, Renew. Sustain. Energy Rev. 52 (2015) 1580–1595, https://doi.org/10.1016/j.rser.2015.07.191.

[9] P. Roy, G. Dias, Prospects for pyrolysis technologies in the bioenergy sector: a review, Renew. Sustain. Energy Rev. 77 (2017) 59–69, https://doi.org/10.1016/j.rser.2017.03.136.

[10] S.P. Sohi, E. Krull, E. Lopez-Capel, R. Bol, Chapter 2 - A review of biochar and its use and function in soil, in: Advances in Agronomy, 105, Academic Press, 2010, pp. 47–82, https://doi.org/10.1016/S0065-2113(10)05002-9.

[11] S. Wang, G. Dai, H. Yang, Z. Luo, Lignocellulosic biomass pyrolysis mechanism: a state-of-the-art review, Prog. Energy Combust. Sci. 62 (2017) 33–86, https://doi.org/10.1016/j.pecs.2017.05.004.

[12] N. Himanshi, Y. Sood, Potential of biochar in improving soil fertility and carbon sequestration, Int. J. Plant Soil Sci. 37 (5) (2025) 609–624, https://doi.org/10.9734/ijpss/2025/v37i55481.

[13] H. Kazemi Shariat Panahi, et al., A comprehensive review of engineered biochar: production, characteristics, and environmental applications, J. Clean. Prod. 270 (2020) 122462, https://doi.org/10.1016/j.jclepro.2020.122462.

[14] J. Lehmann, J. Gaunt, M. Rondon, Bio-char sequestration in terrestrial ecosystems – A review, Mitig. Adapt. Strateg. Glob. Change 11 (2) (2006) 403–427, https://doi.org/10.1007/s11027-005-9006-5.

[15] Y. Li, B. Xing, Y. Ding, X. Han, S. Wang, A critical review of the production and advanced utilization of biochar via selective pyrolysis of lignocellulosic biomass, Bioresour. Technol. 312 (2020) 123614, https://doi.org/10.1016/j.biortech.2020.123614.

[16] J. Maroušek, L. Kolář, M. Vochozka, V. Stehel, A. Marousková, Biochar reduces nitrate level in red beet, Environ. Sci. Pollut. Res. 25 (18) (2018) 18200–18203, https://doi.org/10.1007/s11356-018-2329-z.

[17] D. Woolf, J.E. Amonette, F.A. Street-Perrott, J. Lehmann, S. Joseph, Sustainable biochar to mitigate global climate change, Nat. Commun. 1 (1) (2010) 56, https://doi.org/10.1038/ncomms1053.

[18] Z. Zhang, Z. Zhu, B. Shen, L. Liu, Insights into biochar and hydrochar production and applications: a review, Energy 171 (2019) 581–598, https://doi.org/10.1016/j.energy.2019.01.035.

[19] M. Zhao, et al., Mechanisms of Pb and/or Zn adsorption by different biochars: biochar characteristics, stability, and binding energies, Sci. Total Environ. 717 (2020) 136894, https://doi.org/10.1016/j.scitotenv.2020.136894.

[20] J. Chen, et al., Achieving the simultaneous improvement of degradation, thermal, and mechanical properties of polylactic acid composite films by carbon quantum dots, Compos. Part B Eng. 299 (2025) 112442, https://doi.org/10.1016/j.compositesb.2025.112442.

[21] J. Ren, et al., All-biomass nanocomposite films via facile and sustainable design procedure for thermal management and electromagnetic interference shielding, Adv. Sci. 12 (43) (2025) e10372, https://doi.org/10.1002/advs.202510372.

[22] J. Ren, et al., All-biomass derived nanocomposite films, Nano Lett. 25 (19) (2025) 7810–7817, https://doi.org/10.1021/acs.nanolett.5c00846.

[23] A.C.M. Vilas-Boas, L.A.C. Tarelho, H.S.M. Oliveira, F.G.C.S. Silva, D.T. Pio, M.A. A. Matos, Valorisation of residual biomass by pyrolysis: influence of process conditions on products, Sustain. Energy Fuels 8 (2) (2024) 379–396, https://doi.org/10.1039/D3SE01216F.

[24] T. Aysu, M.M. Küçük, Biomass pyrolysis in a fixed-bed reactor: effects of pyrolysis parameters on product yields and characterization of products, Energy 64 (2014) 1002–1025, https://doi.org/10.1016/j.energy.2013.11.053.

[25] P. Basu, Biomass Gasification and Pyrolysis: Practical Design and Theory, Academic Press, 2010.Available: https://books.google.com.bd/books?id=QSypbUSdkikC.

[26] M. Pala, et al., Recycling of product gas does not affect fast pyrolysis oil yield and composition, J. Anal. Appl. Pyrolysis 148 (2020) 104794, https://doi.org/10.1016/j.jaap.2020.104794.

[27] J.Y. Park, J.-K. Kim, C.-H. Oh, J.-W. Park, E.E. Kwon, Production of bio-oil from fast pyrolysis of biomass using a pilot-scale circulating fluidized bed reactor and its characterization, J. Environ. Manage. 234 (2019) 138–144, https://doi.org/10.1016/j.jenvman.2018.12.104.

[28] C.E. Efika, J.A. Onwudili, P.T. Williams, Influence of heating rates on the products of high-temperature pyrolysis of waste wood pellets and biomass model compounds, Waste Manag. 76 (2018) 497–506, https://doi.org/10.1016/j.wasman.2018.03.021.

[29] N. Gómez, J.G. Rosas, J. Cara, O. Martínez, J.A. Alburquerque, M.E. Sánchez, Slow pyrolysis of relevant biomasses in the Mediterranean basin. Part 1. Effect of temperature on process performance on a pilot scale, J. Clean. Prod. 120 (2016) 181–190, https://doi.org/10.1016/j.jclepro.2014.10.082.

[30] X. Deng, et al., Exploring negative emission potential of biochar to achieve carbon neutrality goal in China, Nat. Commun. 15 (1) (2024) 1085, https://doi.org/10.1038/s41467-024-45314-y.

[31] N. Kaur, C. Kieffer, W. Ren, D. Hui, How much is soil nitrous oxide emission reduced with biochar application? An evaluation of meta-analyses, GCB Bioenergy 15 (1) (2023) 24–37, https://doi.org/10.1111/gcbb.13003.

[32] D.A. Laird, The charcoal vision: a win–Win–Win scenario for simultaneously producing bioenergy, permanently sequestering carbon, while improving soil and water quality, Agron. J. 100 (1) (2008) 178–181, https://doi.org/10.2134/agronj2007.0161.

[33] N.A. Qambrani, MD.M. Rahman, S. Won, S. Shim, C. Ra, Biochar properties and eco-friendly applications for climate change mitigation, waste management, and wastewater treatment: a review, Renew. Sustain. Energy Rev. 79 (2017) 255–273, https://doi.org/10.1016/j.rser.2017.05.057.

[34] R.K. Shrestha, et al., Biochar as a negative emission technology: a synthesis of field research on greenhouse gas emissions, J. Environ. Qual. 52 (4) (2023) 769–798, https://doi.org/10.1002/jeq2.20475.

[35] F. Xia, Z. Zhang, Q. Zhang, H. Huang, X. Zhao, Life cycle assessment of greenhouse gas emissions for various feedstocks-based biochars as soil amendment, Sci. Total Environ. 911 (2024) 168734, https://doi.org/10.1016/j.scitotenv.2023.168734.

[36] Intergovernmental Panel on Climate Change (IPCC), Technical summary. Climate Change 2022 - Mitigation of Climate Change: Working Group III Contribution to the Sixth Assessment Report of the Intergovernmental Panel on Climate Change, Cambridge University Press, Cambridge, 2023, pp. 51–148, https://doi.org/10.1017/9781009157926.002.

[37] M.M. Rahman, M.A. Haque, A.K.M.A. Kabir, M.A. Hashem, M.A.K. Azad, M.K. J. Bhuiyan, Efficacy of biogas production from different types of livestock manures, Int. J. Smart Grid - IjSmartGrid 5 (4) (2021) 158–166.

[38] W. Song, M. Guo, Quality variations of poultry litter biochar generated at different pyrolysis temperatures, J. Anal. Appl. Pyrolysis 94 (2012) 138–145, https://doi.org/10.1016/j.jaap.2011.11.018.

[39] S. Zhang, Q. Dong, L. Zhang, Y. Xiong, Effects of water washing and torrefaction on the pyrolysis behavior and kinetics of rice husk through TGA and Py-GC/MS, Bioresour. Technol. 199 (2016) 352–361, https://doi.org/10.1016/j.biortech.2015.08.110.

[40] B. Bushra, N. Remya, Biochar from pyrolysis of rice husk biomass—characteristics, modification and environmental application, Biomass Convers. Biorefinery 14 (5) (2024) 5759–5770, https://doi.org/10.1007/s13399-020-01092-3.

[41] K. Weiland, et al., Excellence in excrements: upcycling of herbivore manure into nanocellulose and biogas, ACS Sustain. Chem. Eng. 9 (46) (2021) 15506–15513, https://doi.org/10.1021/acssuschemeng.1c05175.

[42] W. Barszcz, M. Łożyńska, J. Molenda, Impact of pyrolysis process conditions on the structure of biochar obtained from apple waste, Sci. Rep. 14 (1) (2024) 10501, https://doi.org/10.1038/s41598-024-61394-8.

[43] S.E. Ibitoye, et al., Design and construction of low-cost biomass pyrolysis reactor for research and teaching in universities and colleges, Biomass Convers.

Biorefinery 15 (12) (2025) 18887–18903, https://doi.org/10.1007/s13399-024-06375-7.
[44] Seetharaman, K. Moorthy, N. Patwa, Saravanan, Y. Gupta, Breaking barriers in deployment of renewable energy, Heliyon 5 (1) (2019) e01166, https://doi.org/10.1016/j.heliyon.2019.e01166.
[45] R. Swaminathan, F.N.P. Nandjembo, Design and testing of a solar torrefaction unit to produce charcoal, J. Sustain. Bioenergy Syst. 06 (3) (2016) 66–71, https://doi.org/10.4236/jsbs.2016.63007.
[46] S. Moorthi, M. Megaraj, Design and development of single screw conveying machine for pyrolysis of waste plastics using nano zeolite particles in fixed bed reactor, Mater. Today Proc. 47 (2021) 880–884, https://doi.org/10.1016/j.matpr.2021.04.126.
[47] A. Dhaundiyal, G. Bercesi, D. Atsu, L. Toth, Development of a small-scale reactor for upgraded biofuel pellets, Renew. Energy 170 (2021) 1197–1214, https://doi.org/10.1016/j.renene.2021.02.057.
[48] C. Caputo, O. Mašek, SPEAR (solar pyrolysis energy access reactor): theoretical design and evaluation of a small-scale low-cost pyrolysis unit for implementation in rural communities, Energies 14 (8) (2021) 2189, https://doi.org/10.3390/en14082189.
[49] M.R. Patel, N.L. Panwar, Development, process optimization and assessment of sustainable mobile biochar kiln for agricultural use, J. Clean. Prod. 477 (2024) 143866, https://doi.org/10.1016/j.jclepro.2024.143866.
[50] D. Woolf, J. Lehmann, S. Joseph, C. Campbell, F.C. Christo, L.T. Angenent, An open-source biomass pyrolysis reactor, Biofuels Bioprod. Biorefining 11 (6) (2017) 945–954, https://doi.org/10.1002/bbb.1814.
[51] W. Jerzak, E. Acha, B. Li, Comprehensive review of biomass pyrolysis: conventional and advanced technologies, reactor designs, product compositions and yields, and techno-economic analysis, Energies 17 (20) (2024) 5082, https://doi.org/10.3390/en17205082.
[52] H. Yang, R. Yan, H. Chen, D.H. Lee, C. Zheng, Characteristics of hemicellulose, cellulose and lignin pyrolysis, Fuel 86 (12) (2007) 1781–1788, https://doi.org/10.1016/j.fuel.2006.12.013.
[53] E. Cárdenas-Aguiar, A. Méndez, G. Gascó, M. Lado, A. Paz-González, The effects of feedstock, pyrolysis temperature, and residence time on the properties and uses of biochar from broom and gorse wastes, Appl. Sci. 14 (10) (2024) 4283, https://doi.org/10.3390/app14104283.
[54] A. Al-Rumaihi, M. Shahbaz, G. Mckay, H. Mackey, T. Al-Ansari, A review of pyrolysis technologies and feedstock: a blending approach for plastic and biomass towards optimum biochar yield, Renew. Sustain. Energy Rev. 167 (2022) 112715, https://doi.org/10.1016/j.rser.2022.112715.
[55] Q. Meng, K. Zhang, R. He, Z. Qu, A review of thermal shock behavior of ceramics: fundamental theory, experimental methods, and outlooks, Int. J. Appl. Ceram. Technol. 21 (6) (2024) 3789–3811, https://doi.org/10.1111/ijac.14846.
[56] L. Zhang, et al., Key issues of MoSi2-UHTC ceramics for ultra high temperature heating element applications: mechanical, electrical, oxidation and thermal shock behaviors, J. Alloys Compd. 780 (2019) 156–163, https://doi.org/10.1016/j.jallcom.2018.11.384.
[57] A. Tomczyk, Z. Sokołowska, P. Boguta, Biochar physicochemical properties: pyrolysis temperature and feedstock kind effects, Rev. Environ. Sci. Biotechnol. 19 (1) (2020) 191–215, https://doi.org/10.1007/s11157-020-09523-3.
[58] Y. Chen, X. Zhang, W. Chen, H. Yang, H. Chen, The structure evolution of biochar from biomass pyrolysis and its correlation with gas pollutant adsorption performance, Bioresour. Technol. 246 (2017) 101–109, https://doi.org/10.1016/j.biortech.2017.08.138.
[59] P. Pariyar, K. Kumari, M.K. Jain, P.S. Jadhao, Evaluation of change in biochar properties derived from different feedstock and pyrolysis temperature for environmental and agricultural application, Sci. Total Environ. 713 (2020) 136433, https://doi.org/10.1016/j.scitotenv.2019.136433.
[60] A. Lataf, et al., The effect of pyrolysis temperature and feedstock on biochar agronomic properties, J. Anal. Appl. Pyrolysis 168 (2022) 105728, https://doi.org/10.1016/j.jaap.2022.105728.
[61] W. Suliman, J.B. Harsh, N.I. Abu-Lail, A.-M. Fortuna, I. Dallmeyer, M. Garcia-Perez, Influence of feedstock source and pyrolysis temperature on biochar bulk and surface properties, Biomass Bioenergy 84 (2016) 37–48, https://doi.org/10.1016/j.biombioe.2015.11.010.
[62] M.H. Samsudin, et al., Economic evaluation of woodchip-derived bio-adsorbent production: a case study using a self-sustained pilot-scale pool-type carbonization reactor, Environ. Sci. Pollut. Res. 32 (34) (2025) 20414–20426, https://doi.org/10.1007/s11356-025-36859-6.
[63] S.S. Harsono, et al., Energy balances, greenhouse gas emissions and economics of biochar production from palm oil empty fruit bunches, Resour. Conserv. Recycl. 77 (2013) 108–115, https://doi.org/10.1016/j.resconrec.2013.04.005.
[64] A. Setiawan, F. Faisal, K. Anshar, R. Hasibuan, S. Riskina, Alchalil, Techno-economic assessment of densified Arabica coffee pulp pyrolysis in a pilot-scale reactor, Biomass Convers. Biorefinery 15 (6) (2025) 9299–9309, https://doi.org/10.1007/s13399-024-05932-4.
[65] R. Bergman, K. Sahoo, K. Englund, S.H. Mousavi-Avval, Lifecycle assessment and techno-economic analysis of biochar pellet production from forest residues and field application, Energies 15 (4) (2022) 1559, https://doi.org/10.3390/en15041559.
[66] T. Haeldermans, L. Campion, T. Kuppens, K. Vanreppelen, A. Cuypers, S. Schreurs, A comparative techno-economic assessment of biochar production from different residue streams using conventional and microwave pyrolysis, Bioresour. Technol. 318 (2020) 124083, https://doi.org/10.1016/j.biortech.2020.124083.
[67] M. Nematian, C. Keske, J.N. Ng'ombe, A techno-economic analysis of biochar production and the bioeconomy for orchard biomass, Waste Manag. 135 (2021) 467–477, https://doi.org/10.1016/j.wasman.2021.09.014.
[68] N. Gautam, M. Athira, K.V. Rose, A. Chaurasia, Study on chemical kinetics and characterization of nanosilica from rice husk and rice straw in the fixed-bed pyrolysis process, Biomass Convers. Biorefinery 12 (5) (2022) 1435–1448, https://doi.org/10.1007/s13399-020-00838-3.
[69] I.F. Titiladunayo, A.G. McDonald, O.P. Fapetu, Effect of temperature on biochar product yield from selected lignocellulosic biomass in a pyrolysis process, Waste Biomass Valorization 3 (3) (2012) 311–318, https://doi.org/10.1007/s12649-012-9118-6.
[70] Y. Nie, et al., Synthesis of mesoporous sulfonated carbon from chicken bones to boost rapid conversion of 5-hydroxymethylfurfural and carbohydrates to 5-ethoxymethylfurfural, Renew. Energy 192 (2022) 279–288, https://doi.org/10.1016/j.renene.2022.04.105.
[71] M. Baniasadi, A. Tugnoli, R. Conti, C. Torri, D. Fabbri, V. Cozzani, Waste to energy valorization of poultry litter by slow pyrolysis, Renew. Energy 90 (2016) 458–468, https://doi.org/10.1016/j.renene.2016.01.018.
[72] S.-S. Kim, F.A. Agblevor, J. Lim, Fast pyrolysis of chicken litter and turkey litter in a fluidized bed reactor, J. Ind. Eng. Chem. 15 (2) (2009) 247–252, https://doi.org/10.1016/j.jiec.2008.10.004.
[73] L.M. Simbolon, D.S. Pandey, A. Horvat, J.J. Leahy, S.A. Tassou, M. Kwapinska, Influence of the pyrolysis temperature on fresh and pelletised chicken litter with focus on sustainable production and utilisation of biochar, Biomass Convers. Biorefinery 14 (20) (2024) 26443–26457, https://doi.org/10.1007/s13399-023-04787-5.
[74] M.A. Atieh, O.Y. Bakather, B. Al-Tawbini, A.A. Bukhari, F.A. Abuilaiwi, M. B. Fettouhi, Effect of carboxylic functional group functionalized on carbon nanotubes surface on the removal of lead from water, Bioinorg. Chem. Appl. 2010 (1) (2010) 603978, https://doi.org/10.1155/2010/603978.
[75] A.K. Mondal, et al., Macroalgae-based biochar: preparation and characterization of physicochemical properties for potential applications, RSC Sustain 2 (6) (2024) 1828–1836, https://doi.org/10.1039/D4SU00008K.
[76] A. Antanasković, et al., Biochar as an enzyme immobilization support and its application for dye degradation, Processes 12 (11) (2024) 2418, https://doi.org/10.3390/pr12112418.
[77] A. Antanasković, et al., Toxic dye removal by thermally modified lignocellulosic waste in a three-phase air-lift reactor: kinetic insights: original scientific paper, Hem. Ind. Chem. Ind. 78 (3) (2024) 241–252, https://doi.org/10.2298/HEMIND230607015A.
[78] T. Aydemir, S. Güler, Characterization and immobilization of Trametes versicolor laccase on magnetic chitosan–clay composite beads for phenol removal, Artif. Cells Nanomedicine Biotechnol. 43 (6) (2015) 425–432, https://doi.org/10.3109/21691401.2015.1058809.
[79] C.H. Chia, B. Gong, S.D. Joseph, C.E. Marjo, P. Munroe, A.M. Rich, Imaging of mineral-enriched biochar by FTIR, Raman and SEM–EDX, Vib. Spectrosc. 62 (2012) 248–257, https://doi.org/10.1016/j.vibspec.2012.06.006.
[80] T. Fazal, et al., Macroalgae and coal-based biochar as a sustainable bioresource reuse for treatment of textile wastewater, Biomass Convers. Biorefinery 11 (5) (2021) 1491–1506, https://doi.org/10.1007/s13399-019-00555-6.
[81] S.M. Salili, A. Ataie, M.R. Barati, Z. Sadighi, Characterization of mechano-thermally synthesized Curie temperature-adjusted La0.8Sr0.2MnO3 nanoparticles coated with (3-aminopropyl) triethoxysilane, Mater. Charact. 106 (2015) 78–85, https://doi.org/10.1016/j.matchar.2015.05.025.
[82] B. Armynah, Z.D. Atika, W.H. Piarah, D. Tahir, Analysis of chemical and physical properties of biochar from rice husk biomass, J. Phys. Conf. Ser. 979 (1) (2018) 012038, https://doi.org/10.1088/1742-6596/979/1/012038.
[83] S.-C. Her, C.-Y. Lai, Dynamic behavior of nanocomposites reinforced with multi-walled carbon nanotubes (MWCNTs), Materials (Basel) 6 (6) (2013) 2274–2284, https://doi.org/10.3390/ma6062274.
[84] M. Keiluweit, P.S. Nico, M.G. Johnson, M. Kleber, Dynamic molecular structure of plant biomass-derived black carbon (Biochar), Environ. Sci. Technol. 44 (4) (2010) 1247–1253, https://doi.org/10.1021/es9031419.
[85] Z. Ding, Y. Wan, X. Hu, S. Wang, A.R. Zimmerman, B. Gao, Sorption of lead and methylene blue onto hickory biochars from different pyrolysis temperatures: importance of physicochemical properties, J. Ind. Eng. Chem. 37 (2016) 261–267, https://doi.org/10.1016/j.jiec.2016.03.035.
[86] G. Mujtaba, R. Hayat, Q. Hussain, M. Ahmed, Physio-chemical characterization of biochar, compost and Co-composted biochar derived from green waste, Sustainability 13 (9) (2021) 4628, https://doi.org/10.3390/su13094628.
[87] S. Haghighi Mood, M. Ayiania, H. Cao, O. Marin-Flores, Y.J. Milan, M. Garcia-Perez, Nitrogen and magnesium Co-doped biochar for phosphate adsorption, Biomass Convers. Biorefinery 14 (5) (2024) 5923–5942, https://doi.org/10.1007/s13399-021-01404-1.
[88] A.F. Martins, J. Diniz, J.A. Stahl, A. de L. Cardoso, Caracterização dos produtos líquidos e do carvão da pirólise de serragem de eucalipto, Quím. Nova 30 (2007) 873–878, https://doi.org/10.1590/S0100-40422007000400021.
[89] J. Dias, A. Conceição, F.M. Delatorre, P. Siqueira, Production, characterization physical, chemical, and structural analysis of biochar fines for bio-reinforcement in composite materials, Processes 13 (2) (2025) 504, https://doi.org/10.3390/pr13020504.
[90] J.E. Kim, et al., Adsorptive removal of tetracycline from aqueous solution by maple leaf-derived biochar, Bioresour. Technol. 306 (2020) 123092, https://doi.org/10.1016/j.biortech.2020.123092.
[91] M. Thommes, et al., Physisorption of gases, with special reference to the evaluation of surface area and pore size distribution (IUPAC Technical Report),

Pure Appl. Chem. 87 (9–10) (2015) 1051–1069, https://doi.org/10.1515/pac-2014-1117.
[92] M. Kalina, et al., Biochar texture—a parameter influencing physicochemical properties, morphology, and agronomical potential, Agronomy 12 (8) (2022) 1768, https://doi.org/10.3390/agronomy12081768.
[93] N. Li, Q. Xia, M. Niu, Q. Ping, H. Xiao, Immobilizing laccase on different species wood biochar to remove the chlorinated biphenyl in wastewater, Sci. Rep. 8 (1) (2018) 13947, https://doi.org/10.1038/s41598-018-32013-0.
[94] J. Kujawska, E. Wojtaś, B. Charmas, Biochar derived from sewage sludge: the impact of pyrolysis temperature on chemical properties and agronomic potential, Sustainability 16 (18) (2024) 8225, https://doi.org/10.3390/su16188225.
[95] A. Wang, et al., Environmental risk assessment in livestock manure derived biochars, RSC Adv 9 (69) (2019) 40536–40545, https://doi.org/10.1039/C9RA08186K.
[96] A. Wang, et al., Speciation and environmental risk of heavy metals in biochars produced by pyrolysis of chicken manure and water-washed swine manure, Sci. Rep. 11 (1) (2021) 11994, https://doi.org/10.1038/s41598-021-91440-8.
[97] X. Wang, Q. Chi, X. Liu, Y. Wang, Influence of pyrolysis temperature on characteristics and environmental risk of heavy metals in pyrolyzed biochar made from hydrothermally treated sewage sludge, Chemosphere 216 (2019) 698–706, https://doi.org/10.1016/j.chemosphere.2018.10.189.
[98] A.V. Bridgwater, Review of fast pyrolysis of biomass and product upgrading, Biomass Bioenergy 38 (2012) 68–94, https://doi.org/10.1016/j.biombioe.2011.01.048.
[99] J.A. Onwudili, C.A. Scaldaferri, Catalytic upgrading of intermediate pyrolysis bio-oil to hydrocarbon-rich liquid biofuel via a novel two-stage solvent-assisted process, Fuel 352 (2023) 129015, https://doi.org/10.1016/j.fuel.2023.129015.
[100] Q. Zhang, J. Chang, T. Wang, Y. Xu, Review of biomass pyrolysis oil properties and upgrading research, Energy Convers. Manag. 48 (1) (2007) 87–92, https://doi.org/10.1016/j.enconman.2006.05.010.
[101] O.D. Mante, F.A. Agblevor, Storage stability of biocrude oils from fast pyrolysis of poultry litter, Waste Manag. 32 (1) (2012) 67–76, https://doi.org/10.1016/j.wasman.2011.09.004.
[102] C.M. Monreal, M. Schnitzer, Production of a refined biooil derived by fast pyrolysis of chicken manure with chemical and physical characteristics close to those of fossil fuels, J. Environ. Sci. Health Part B 46 (7) (2011) 630–637, https://doi.org/10.1080/03601234.2011.594377.
[103] M.Z.H. Khan, M. Sultana, M.R. Al-Mamun, M.R. Hasan, Pyrolytic waste plastic oil and its diesel blend: fuel characterization, J. Environ. Public Health (1) (2016) 1–6, https://doi.org/10.1155/2016/7869080.
[104] D. Bisen, R. Lanjewar, A.P.S. Chouhan, M. Pant, S. Chakma, Catalytic co-pyrolysis of rice husk and high-density polyethylene using dolomite for enhancement of bio-oil production and quality, Environ. Sci. Pollut. Res. 32 (26) (2025) 15676–15694, https://doi.org/10.1007/s11356-025-36600-3.
[105] A. Ben Hassen-Trabelsi, T. Kraiem, S. Naoui, H. Belayouni, Pyrolysis of waste animal fats in a fixed-bed reactor: production and characterization of bio-oil and bio-char, Waste Manag. 34 (1) (2014) 210–218, https://doi.org/10.1016/j.wasman.2013.09.019.
[106] D. Makenov, et al., Evaluation of vacuum residue decomposition kinetics with a catalyst by thermogravimetric analysis, Catalysts 15 (5) (2025) 493, https://doi.org/10.3390/catal15050493.
[107] L. Maulinda, et al., The influence of pyrolysis time and temperature on the composition and properties of bio-oil prepared from Tanjong leaves (Mimusops elengi), Sustainability 15 (18) (2023) 13851, https://doi.org/10.3390/su151813851.
[108] C. Paenpong, A. Pattiya, Effect of pyrolysis and moving-bed granular filter temperatures on the yield and properties of bio-oil from fast pyrolysis of biomass, J. Anal. Appl. Pyrolysis 119 (2016) 40–51, https://doi.org/10.1016/j.jaap.2016.03.019.
[109] S. Stegen, P. Kaparaju, Effect of temperature on oil quality obtained through pyrolysis of sugarcane bagasse, Fuel 276 (2020) 118112, https://doi.org/10.1016/j.fuel.2020.118112.
[110] Y. Jin, et al., Numerical simulation of solar-driven biomass pyrolysis for structured biochar production, Energy 342 (2026) 139733, https://doi.org/10.1016/j.energy.2025.139733.
[111] R. Pan, et al., Enhancing carbon nanotubes production from pyrolysis-catalysis of plastic waste through monolithic heating, Natl. Sci. Rev. (2026) nwag143, https://doi.org/10.1093/nsr/nwag143.
[112] J. Liu, et al., Biomass pyrolysis mechanism for carbon-based high-value products, Proc. Combust. Inst. 39 (3) (2023) 3157–3181, https://doi.org/10.1016/j.proci.2022.09.063.
[113] S. Somboon, et al., Transformations in physicochemical properties and pore structure of biochar derived from rice straw revealed by synchrotron techniques, Sci. Rep. 15 (1) (2025) 23641, https://doi.org/10.1038/s41598-025-08772-y.
[114] Z. Khan, et al., Compensation of high nitrogen toxicity and nitrogen deficiency with biochar amendment through enhancement of soil fertility and nitrogen use efficiency promoted rice growth and yield, GCB Bioenergy 13 (11) (2021) 1765–1784, https://doi.org/10.1111/gcbb.12884.
[115] C.X. Sun, X. Chen, M.M. Cao, M.Q. Li, Y.L. Zhang, Growth and metabolic responses of maize roots to straw biochar application at different rates, Plant Soil 416 (1) (2017) 487–502, https://doi.org/10.1007/s11104-017-3229-6.
[116] S. Zhang, et al., Effect of biochar on biochemical properties of saline soil and growth of rice, Heliyon 10 (1) (2024) e23859, https://doi.org/10.1016/j.heliyon.2023.e23859.
[117] L. Lai, M.R. Ismail, F.M. Muharam, M.M. Yusof, R. Ismail, N.M. Jaafar, Effects of rice straw biochar and nitrogen fertilizer on rice growth and yield, Asian J. Crop Sci. 9 (4) (2017) 159–166.
[118] B. Liu, H. Li, H. Li, A. Zhang, Z. Rengel, Long-term biochar application promotes rice productivity by regulating root dynamic development and reducing nitrogen leaching, GCB Bioenergy 13 (1) (2021) 257–268, https://doi.org/10.1111/gcbb.12766.
[119] N. An, et al., Biochar application with reduced chemical fertilizers improves soil pore structure and rice productivity, Chemosphere 298 (2022) 134304, https://doi.org/10.1016/j.chemosphere.2022.134304.
[120] W. Gu, et al., Long-term effects of biochar application with reduced chemical fertilizer on paddy soil properties and japonica rice production system, Front. Environ. Sci. 10 (2022), https://doi.org/10.3389/fenvs.2022.902752.
[121] Q. Zhang, et al., Effects of six-year biochar amendment on soil aggregation, crop growth, and nitrogen and phosphorus use efficiencies in a rice-wheat rotation, J. Clean. Prod. 242 (2020) 118435, https://doi.org/10.1016/j.jclepro.2019.118435.
[122] W.A.M.A.N. Illankoon, et al., Development of a dual-chamber pyrolizer for biochar production from agricultural waste in Sri Lanka, Energies 16 (4) (2023) 1819, https://doi.org/10.3390/en16041819.
[123] K.F. Adoko, P.D. Kombienou, H.A. Azontondé, W. Cornelis, Development of a pilot kiln and characterization of biochars for agricultural use and carbon sequestration in Benin, Biomass Bioenergy 206 (2026) 108666, https://doi.org/10.1016/j.biombioe.2025.108666.
[124] S.G. Asabie, B.T. Admasu, Design, fabrication, and performance evaluation of a pyrolysis reactor for charcoal production from eucalyptus. Comparison to traditional earth kiln method in Ethiopia, Results Eng. 28 (2025) 107379, https://doi.org/10.1016/j.rineng.2025.107379.